



**NAVAL  
POSTGRADUATE  
SCHOOL**

**MONTEREY, CALIFORNIA**

**THESIS**

**SYNTHESIS AND CHARACTERIZATION OF NITROGEN-  
DOPED GRAPHENE**

by

D. Ryan Palaniuk

September 2012

Thesis Advisor:  
Second Reader:

Claudia Luhrs  
Sebastian Osswald

**Approved for public release; distribution is unlimited**

THIS PAGE INTENTIONALLY LEFT BLANK

REPORT DOCUMENTATION PAGE			Form Approved OMB No. 0704-0188	
Public reporting burden for this collection of information is estimated to average 1 hour per response, including the time for reviewing instruction, searching existing data sources, gathering and maintaining the data needed, and completing and reviewing the collection of information. Send comments regarding this burden estimate or any other aspect of this collection of information, including suggestions for reducing this burden, to Washington headquarters Services, Directorate for Information Operations and Reports, 1215 Jefferson Davis Highway, Suite 1204, Arlington, VA 22202-4302, and to the Office of Management and Budget, Paperwork Reduction Project (0704-0188) Washington DC 20503.				
1. AGENCY USE ONLY (Leave blank)		2. REPORT DATE September 2012	3. REPORT TYPE AND DATES COVERED Master's Thesis	
4. TITLE AND SUBTITLE Synthesis and Characterization of Nitrogen-Doped Graphene			5. FUNDING NUMBERS	
6. AUTHOR(S) D. Ryan Palaniuk				
7. PERFORMING ORGANIZATION NAME(S) AND ADDRESS(ES) Naval Postgraduate School Monterey, CA 93943-5000			8. PERFORMING ORGANIZATION REPORT NUMBER	
9. SPONSORING /MONITORING AGENCY NAME(S) AND ADDRESS(ES) N/A			10. SPONSORING/MONITORING AGENCY REPORT NUMBER	
11. SUPPLEMENTARY NOTES The views expressed in this thesis are those of the author and do not reflect the official policy or position of the Department of Defense or the U.S. Government. IRB Protocol number _____N/A_____.				
12a. DISTRIBUTION / AVAILABILITY STATEMENT Approved for public release; distribution is unlimited			12b. DISTRIBUTION CODE A	
13. ABSTRACT (maximum 200 words) Self standing nitrogen doped graphene sheets were produced by reduction-expansion method, which utilizes graphite oxide (GO) and urea as precursor materials. For comparison, an Atmospheric Microwave Plasma Torch system (ATP) was used to produce graphene samples under argon and nitrogen atmospheres from GO. Graphene samples were characterized by XRD, TEM, SEM, BET and Raman Spectroscopy. The GO and urea mixtures decomposition-reduction process, as well as nitrogen doped graphene stability at high temperatures, were studied by TGA/DSC analysis. Results indicate that the amount of nitrogen introduced into the graphene structure can be controlled by varying the initial amount of urea in precursor mixtures. Reduction-expansion method provides a pathway to generate nitrogen doped graphene by a process that is rapid, inexpensive and easy to scale up. Plasma produced graphene samples show higher surface areas than reduction-expansion produced samples, although no evidence was found of nitrogen doping by the use of nitrogen atmospheres under the plasma experimental conditions used. Resulting nitrogen doped self standing graphene sheets from reduction-expansion protocols are potential candidates to be used as ultracapacitor and battery electrodes.				
14. SUBJECT TERMS graphene, carbon, nitrogen, doped, ultracapacitor, supercapacitor, electrode			15. NUMBER OF PAGES 79	
			16. PRICE CODE	
17. SECURITY CLASSIFICATION OF REPORT Unclassified	18. SECURITY CLASSIFICATION OF THIS PAGE Unclassified	19. SECURITY CLASSIFICATION OF ABSTRACT Unclassified	20. LIMITATION OF ABSTRACT UU	

THIS PAGE INTENTIONALLY LEFT BLANK

**Approved for public release; distribution is unlimited**

**SYNTHESIS AND CHARACTERIZATION OF NITROGEN-DOPED  
GRAPHENE**

D. Ryan Palaniuk  
Lieutenant, United States Navy  
B.S., University of Idaho, 2005

Submitted in partial fulfillment of the  
requirements for the degree of

**MASTER OF SCIENCE IN ENGINEERING SCIENCES**

from the

**NAVAL POSTGRADUATE SCHOOL  
September 2012**

Author: D. Ryan Palaniuk

Approved by: Claudia Luhrs  
Thesis Advisor

Sebastian Osswald  
Thesis Second Reader

Knox Millsaps  
Chair, Department of Mechanical and Aerospace Engineering

THIS PAGE INTENTIONALLY LEFT BLANK

## ABSTRACT

Self-standing nitrogen-doped graphene was produced by reduction-expansion method, which utilizes graphite oxide (GO) and urea as precursor materials. For comparison, an Atmospheric Microwave Plasma Torch system (ATP) was used to produce graphene samples from GO under argon and nitrogen atmospheres. Graphene samples were characterized by X-Ray Diffraction, Transmission Electron Microscopy, Scanning Electron Microscopy, Brunauer-Emmet-Teller analysis and Raman Spectroscopy. The GO and urea mixtures decomposition-reduction process, as well as nitrogen doped graphene stability at high temperatures, were studied by TGA/DSC analysis. Results indicate that the amount of nitrogen introduced into the graphene structure can be controlled by varying the initial amount of urea in precursor mixtures. Reduction-expansion method provides a pathway to generate nitrogen doped graphene by a process that is rapid, inexpensive and easy to scale up. Plasma produced graphene samples show higher surface areas than reduction-expansion produced samples, although no evidence was found of nitrogen doping by the use of nitrogen atmospheres under the plasma experimental conditions used. Resulting nitrogen doped self-standing graphene sheets from reduction-expansion protocols are potential candidates to be used as ultracapacitor and battery electrodes.

THIS PAGE INTENTIONALLY LEFT BLANK

# TABLE OF CONTENTS

<b>I.</b>	<b>INTRODUCTION.....</b>	<b>1</b>
<b>A.</b>	<b>ULTRACAPACITOR ELECTRODES.....</b>	<b>1</b>
<b>B.</b>	<b>GRAPHENE.....</b>	<b>5</b>
<b>C.</b>	<b>THESIS OBJECTIVE.....</b>	<b>8</b>
<b>D.</b>	<b>HYPOTHESIS.....</b>	<b>8</b>
<b>II.</b>	<b>EXPERIMENTAL METHODS.....</b>	<b>10</b>
<b>A.</b>	<b>GRAPHENE PRODUCTION BACKGROUND.....</b>	<b>10</b>
<b>B.</b>	<b>PRODUCTION OF GRAPHITIC OXIDE.....</b>	<b>12</b>
<b>C.</b>	<b>PRODUCTION OF NITROGEN-DOPED GRAPHENE.....</b>	<b>13</b>
<b>1.</b>	<b>Method 1: Expansion-Reduction.....</b>	<b>13</b>
<b>2.</b>	<b>Method 2: Aerosol-Through-Plasma (ATP).....</b>	<b>15</b>
<b>III.</b>	<b>CHARACTERIZATION.....</b>	<b>19</b>
<b>A.</b>	<b>X-RAY DIFFRACTION.....</b>	<b>19</b>
<b>1.</b>	<b>Purpose.....</b>	<b>19</b>
<b>2.</b>	<b>Testing Parameters.....</b>	<b>20</b>
<b>B.</b>	<b>BET ANALYSIS.....</b>	<b>21</b>
<b>1.</b>	<b>Purpose.....</b>	<b>21</b>
<b>2.</b>	<b>Testing Parameters.....</b>	<b>22</b>
<b>C.</b>	<b>RAMAN SPECTROSCOPY.....</b>	<b>24</b>
<b>1.</b>	<b>Purpose.....</b>	<b>24</b>
<b>2.</b>	<b>Testing Parameters.....</b>	<b>24</b>
<b>D.</b>	<b>SCANNING ELECTRON MICROSCOPE.....</b>	<b>25</b>
<b>1.</b>	<b>Purpose.....</b>	<b>25</b>
<b>2.</b>	<b>Testing Parameters.....</b>	<b>26</b>
<b>E.</b>	<b>THERMOGRAVIMETRIC ANALYSIS.....</b>	<b>28</b>
<b>1.</b>	<b>Purpose.....</b>	<b>28</b>
<b>2.</b>	<b>Testing Parameters.....</b>	<b>28</b>
<b>F.</b>	<b>MASS SPECTROMETRY.....</b>	<b>30</b>
<b>1.</b>	<b>Purpose.....</b>	<b>30</b>
<b>2.</b>	<b>Testing Parameters.....</b>	<b>31</b>
<b>IV.</b>	<b>RESULTS AND DISCUSSION.....</b>	<b>34</b>
<b>A.</b>	<b>X-RAY DIFFRACTION.....</b>	<b>34</b>
<b>B.</b>	<b>BET ANALYSIS.....</b>	<b>38</b>
<b>C.</b>	<b>RAMAN SPECTROSCOPY.....</b>	<b>39</b>
<b>D.</b>	<b>SCANNING ELECTRON MICROSCOPE.....</b>	<b>40</b>
<b>E.</b>	<b>THERMOGRAVIMETRIC ANALYSIS.....</b>	<b>43</b>
<b>F.</b>	<b>MASS SPECTROSCOPY.....</b>	<b>44</b>
<b>V.</b>	<b>SUMMARY AND CONCLUSIONS.....</b>	<b>48</b>
	<b>LIST OF REFERENCES.....</b>	<b>51</b>
	<b>INITIAL DISTRIBUTION LIST.....</b>	<b>57</b>



THIS PAGE INTENTIONALLY LEFT BLANK

## LIST OF FIGURES

Figure 1.	Diagram our group developed showing how an ultracapacitor functions. A charge forms in an electrode's surface as well as from electrolyte ions moving to each electrode. Thus a "double layer" charge is established. ....2	2
Figure 2.	Ragone plot comparing Energy Density vs Power Density of various energy storage devices. Taken from reference 8. ....4	4
Figure 3.	Some of the different forms graphene can take: a) single sheet of graphene b) buckyballs, c) nanotube, d) graphite. Taken from reference 14. ....6	6
Figure 4.	Overall process of the expansion-reduction method. GO and urea are crushed together in a mortar to form a GO+urea mixture. The mixture is then rapidly heated in a furnace under an inert gas. The result is self-standing graphene sheets where most of the oxygen groups have been removed and (we believe) nitrogen inserted into the lattice. ....14	14
Figure 5.	Picture of furnace with quartz tube. ....15	15
Figure 6.	Schematic of the microwave atmospheric torch system used to produce graphene from GO. Taken from reference 33. ....16	16
Figure 7.	Photograph of a Phillips PW1830 Diffractometer. ....20	20
Figure 8.	Diagram of a NOVAe Series Surface Area Analyzer. Taken from reference 37. ....23	23
Figure 9.	Photograph of a Renishaw inVia Raman Microscope. ....25	25
Figure 10.	Photograph of a Zeiss NEON 40 field emission SEM Microscope. ....27	27
Figure 11.	Photograph of the NETZSCH STA 449 F3 Jupiter Thermal Analyzer. ....29	29
Figure 12.	Diagram of a basic quadrupole mass analyzer configuration. Taken from reference 44. ....31	31
Figure 13.	Diagram showing how rods are electrically connected inside a quadrupole mass analyzer. Taken from reference 44. ....31	31
Figure 14.	Photograph of the NETZSCH QMS 403 C <i>Aëolos</i> Quadrupole Mass Spectrometer (device on the left connection) linked to the NETZSCH STA 449 F3 Jupiter Thermal Analyzer (device on the right connection). ....32	32
Figure 15.	XRD results from analysis with an empty sample disc. ....34	34
Figure 16.	XRD results from analysis of unaltered GO. ....34	34
Figure 17.	XRD results from analysis of thermally expanded GO without urea. ....35	35
Figure 18.	XRD results from analysis of all expansion-reduction prepared samples overlaid with thermally expanded (TE) GO without urea and unaltered GO. ....36	36
Figure 19.	On the left: a comparison of various sample's primary peak position. An increase in urea corresponds to a greater shift to the right. On the right: a comparison of various sample's peak intensity. Intensity reaches a maximum for R=1.25, after which a greater amount of urea leads to a lower intensity. TE for both graphs stands for thermally expanded. ....36	36
Figure 20.	XRD results for both ATP prepared samples. The primary peak that occurs at $26^\circ 2\theta$ is unaltered even after adding nitrogen in aerosol mixture. This suggests that no nitrogen was inserted into the resultant graphene. ....37	37

Figure 21.	Comparison of surface area for different expansion-reduction prepared samples. The thermally expanded (TE) sample, in which no urea was used, shows the largest surface area. ....	38
Figure 22.	On the left: Raman spectrum showing the D/G ratio of various nitrogen-doped samples. On the right: graph showing a relatively linear relationship between D/G ratio and GO:Urea ratio. ....	40
Figure 23.	Two SEM images of unaltered GO. Image on left is at 15K magnification. Image on right is at 60K magnification. ....	40
Figure 24.	SEM images of thermally expanded GO at 15K. Like the unaltered GO, it shows a somewhat loose configuration even though most of the oxygen has been removed. ....	41
Figure 25.	SEM images of three different graphene samples. From top to bottom: R=1.67, R=1.25 and R=1. All images are at 15K magnification. ....	42
Figure 26.	TGA graph showing samples produced from both the expansion-reduction method and the ATP method. The thermally expanded (TE) sample (which was prepared with no urea) and the ATP samples were burned off at a lower temperature than the expansion-reduction samples prepared with urea. All samples were stable up to at least 450° C. ....	43
Figure 27.	TGA graph of ATP sample prepared with argon gas only. The step-down shape is characteristic of unaltered GO. ....	44
Figure 28.	Mass Spectra graph for expansion-reduction sample with an R value of 1 (equal parts GO and urea). ....	45
Figure 29.	Chart showing how much of mass 30 is present in a sample relative to how much of mass 44 is present. There appears to be a loose correlation between the relative amount of Mass 30 (associated with nitrogen molecules) in a sample and the amount of urea used in that sample's preparation. ....	46

THIS PAGE INTENTIONALLY LEFT BLANK

## LIST OF TABLES

Table 1.	Shows the approximate weights of GO and urea used to prepare each sample and the result weight of the product. ....	14
Table 2.	Shows the weight of the GO precursor used and the weight of the product...	17

THIS PAGE INTENTIONALLY LEFT BLANK

## LIST OF ACRONYMS AND ABBREVIATIONS

Å	Angstrom
ATP	Aerosol-Through-Plasma
BET	Brunauer-Emmet-Teller
DSC	Differential Scanning Calorimetry
GO	Graphitic Oxide
MS	Mass Spectroscopy
N-doped	Nitrogen Doped
nm	Nanometer
SEM	Scanning Electron Microscope
TE	Thermally Expanded Graphene
TEM	Transmission Electron Microscope
TGA	Thermogravimetric Analysis
TPO	Temperature Programmed Oxidation
XRD	X-Ray Diffraction
µm	Micrometer

THIS PAGE INTENTIONALLY LEFT BLANK

## EXECUTIVE SUMMARY

The Navy is rapidly adopting the use of unmanned vehicles as versatile tools to achieve national defense goals. These new platforms demand an energy source that must be long-lasting, quickly supplying power to any number of loads and work under a wide variety of conditions. Batteries (which use a chemical reaction to store energy) are already a well-known and widely used portable power source. However, another energy storage device exists that has advantages over batteries and may be well suited to requirements of unmanned vehicles: ultracapacitors.

Ultracapacitors have many advantages over batteries; the most important is that they have a much higher power density. Unfortunately, they have a lower energy density. Researchers are looking for ways to improve ultracapacitors' energy densities. One way to do that is to select an ideal electrode material.

Graphene is particularly well-suited for such a material. In its pristine state, it already possesses necessary traits such as a high surface area and high energy density. However, it may be possible to improve the use of graphene as an electrode material by doping it with nitrogen. The addition of nitrogen could improve graphene's conductivity which could, in turn, improve its ability to store energy.

The primary objective of this work is to develop a scalable method that allows for nitrogen-doping of graphene. The as-produced samples will be analyzed using a variety of different characterization techniques such as XRD, BET, Raman, SEM, TGA and mass spectra to validate doping methods by determining nitrogen levels.

THIS PAGE INTENTIONALLY LEFT BLANK

## ACKNOWLEDGMENTS

First and foremost, I would like to thank my thesis advisor, Dr. Claudia Luhrs. The help and direction she provided on this fascinating, yet difficult, subject was invaluable. She patiently guided me and explained concepts every step of the way. Without her help I could never have completed this thesis or have won the NPS Ralph Krause Materials Research Award for presenting my thesis at the Electronic Materials Symposium. Her wealth of knowledge and method of teaching instilled in me an enthusiasm for this topic, igniting an interest that will carry over throughout the rest of my career.

I also would like to thank Dr. Sebastian Osswald for being my second reader and all the help he provided with Raman spectroscopy. His insight, dedication and skill were of great help to me and resulted in some of the most conclusive findings over the course of working on this subject.

Dr. Sarath Menon was a huge help during my entire time at NPS. Both as a professor inside the classroom and as an instructor for important instruments like the X-Ray Diffractometer and the Scanning Electron Microscope. Thank you for all the time you were willing to you took to train me.

Dr. Chanman Park provided help and lab support almost every step of the way and made it possible to conduct the research presented in this thesis. Thank you.

There are also fellow students who were of great help to me while working on this thesis. LT Ashley Maxson and ENS Michael Moberg both helped me with sample preparations as well as being great in-class lab partners. LT Michael Mowry helped provide extra insight into the workings of the TGA and mass spectrometry analysis, along with Raman spectroscopy. His help and sharp thinking as a fellow Undersea Warfare student was absolutely critical to any success I've had at NPS.

THIS PAGE INTENTIONALLY LEFT BLANK

# I. INTRODUCTION

## A. ULTRACAPACITOR ELECTRODES

The U.S. Navy is rapidly accepting unmanned vehicles as mission platform tools. The National Research Council stressed the importance for the Navy to pursue autonomous vehicles and related technologies [1]. Unmanned vehicles can support a wide range of operations, including: deploy/retrieve devices, data collection/transmission and engagement of air, surface or underwater targets [2]. However, unmanned vehicles have limitations, not the least of which is endurance in the environment in which they operate. Perhaps the single biggest factor affecting endurance is energy.

Vehicles engaged in future high speed and endurance missions will require more sophisticated energy systems [2]. When designing unmanned vehicles with efficiency in mind, it is important to minimize the size, cost and signature of the energy system. This is especially true for underwater vehicles which require air-independent propulsion. An ideal energy storage device for these vehicles should provide high levels of power, have a long service life, be durable under a wide range of environmental conditions, be low weight, require little to no maintenance and be able to recharge very quickly. Moreover, for any expeditionary operations that require the use of handheld or other transportable electronics, the use of energy storage systems is indispensable. Ultracapacitors show promise of meeting all of these requirements.

Ultracapacitors are electrical energy storage devices, based on electrochemical double layer capacitance (EDLC) [3]. A simple capacitor consists of two electrodes (typically two metal plates) separated by a dielectric (an insulator that can be polarized). When charging, a potential is created between the two electrodes. This potential remains (assuming no leakage) until a path is made for the electrons to travel and the capacitor can discharge its energy [4]. In contrast, an ultracapacitor is made of two electrodes that are immersed in an electrolyte that consists of an equal amount of positive and negatively charged ions. When a voltage is induced on an ultracapacitor, each electrode develops a charge (one is negative and the other is positive—as in a simple capacitor). However, as

the charge builds, ions from the electrolyte travel to each electrode. When the ultracapacitor discharges, the ions are no longer attracted to each electrode and return to a uniform distribution. Thus, an ultracapacitor can produce energy when each electrode discharges, but *also* produces energy as the electrolyte ions move away from the electrodes. This effectively means that an EDLC is two capacitors in a series [4].

Another way to think about an EDLC is to imagine two electrodes, connected to an energy source, placed in an electrolyte and separated by a membrane. When a current path is established between the electrodes there is a charge separation at the liquid-solid interface. Energy is stored in the system when current stops flowing as long as the voltage persists. There now exists two parallel liquid-solid interfaces where ions in the electrolyte can attach themselves to—effectively making a double layer (see figure 1).

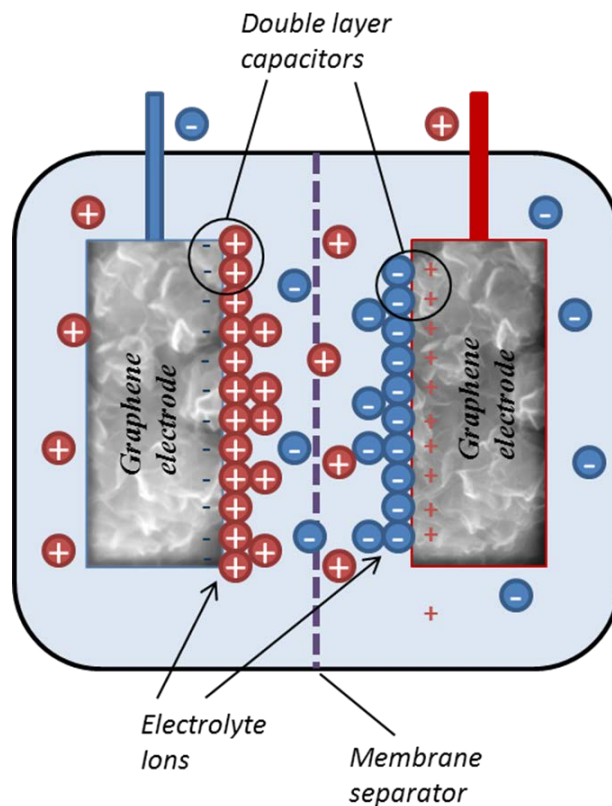


**Figure 1.** Diagram our group developed showing how an ultracapacitor functions. A charge forms in an electrode's surface as well as from electrolyte ions moving to each electrode. Thus a "double layer" charge is established.

Ultracapacitors can store much more energy than a simple capacitor (up to two orders of magnitude) [4]. They are able to do this because energy stored is inversely proportional to separation between the two electrodes [3]. Electrodes in an ultracapacitor are usually much closer (measured in nanometers) versus electrodes in a simple capacitor (usually measured in microns) [4]. This means that the energy density of ultracapacitors is extremely high in comparison to simple capacitors.

However, while ultracapacitors have a clear advantage over simple capacitors, they have certain trade-offs when compared to batteries that store energy in a chemical reaction. Indeed, conventional batteries have many advantages over ultracapacitors. Despite ultracapacitors' high level of energy density versus simple capacitors, they are still much lower than batteries, around an order of magnitude lower [5]. They also have a high level of dielectric absorption (will not completely discharge when given the opportunity) and a high level of self-discharge (internal charge is reduced even before a discharge occurs) [6]. Also, unlike batteries, the voltage of ultracapacitors changes as it discharges, requiring extra devices to smooth the voltage rate and subsequently results in an even greater loss of energy [7].

However, ultracapacitors have advantages over conventional batteries. Ultracapacitors have a much higher rate of power density versus batteries [4]. This means that they charge and discharge much faster when compared to a battery. Other advantages are a longer cycle life, low weight and low maintenance requirements [3]. Since it doesn't require an electrochemical reaction to produce energy, ultracapacitors can function within a greater temperature range [3]. This also means that an ultracapacitor cannot be overcharged.

Figure 2 is of a Ragone plot with some typical energy storage devices. Ragone plots compare energy density versus power density.

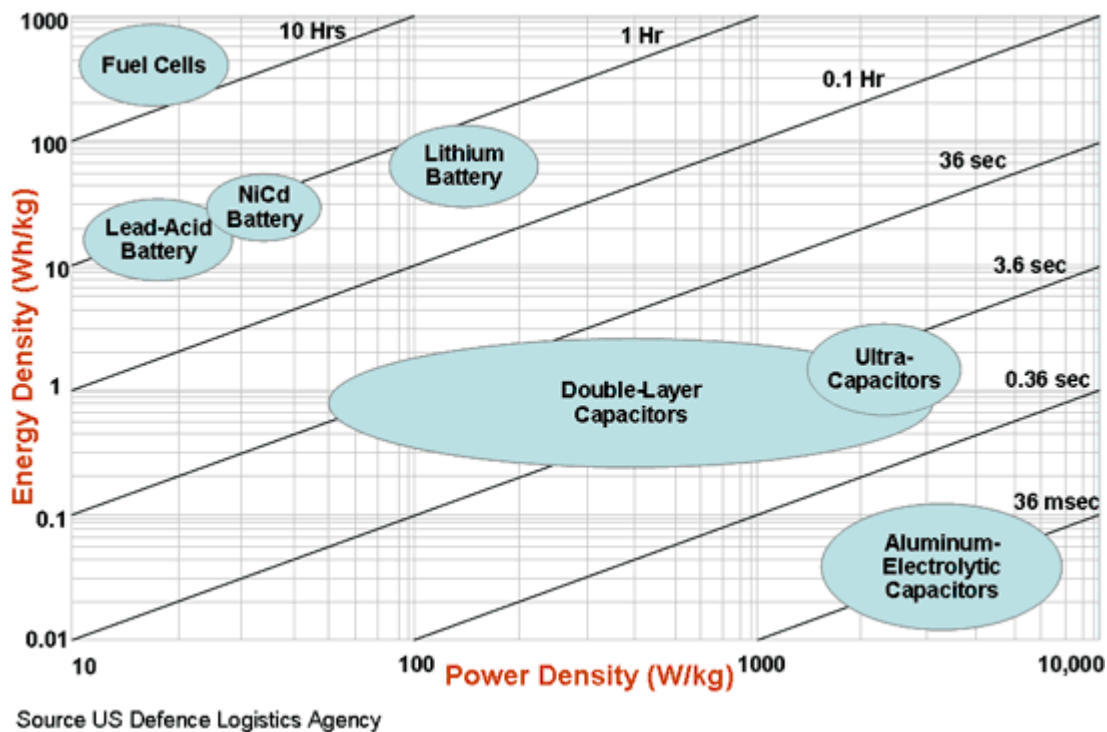


Figure 2. Ragone plot comparing Energy Density vs Power Density of various energy storage devices. Taken from reference 8.

An important feature of an ultracapacitor electrode material is a high surface area. Ultracapacitor electrodes with a high surface area mean that more ions from an electrolyte can cling to it. So, upon discharging, more ions move away from the electrode. This gives the ultracapacitor a greater energy density [4]. Various materials are currently being considered for use in ultracapacitors. Carbon nanotubes have a high surface area due to their large surface-to-volume ratio and may offer additional porosity when arranged properly, allowing for substantial improvements in capacity [9],[10]. Multi-walled carbon nanotubes have an even greater capacity for storing energy versus single-walled nanotubes [11]. A carbon-based aerogel (a composite material) also provides a large surface area (in fact, it's higher per unit volume than any other solid) [12]. Unfortunately, they can only operate at a few volts and have a rather unimpressive energy density in comparison to graphene (90 Wh/kg) [12]. Additional materials are consolidated amorphous carbon (carbon without a particular crystalline structure) and

mineral-based carbon (nonactivated carbon that is synthesized with metals)—also known as carbide-derived carbon [13].

There is another particularly promising material that holds great interest for us. That material is graphene.

## **B. GRAPHENE**

Graphene is a material composed solely of  $sp^2$ -bonded carbon atoms that are arranged in a single layer honeycomb lattice. Because graphene is only a few atomic layers thick, it is considered a two-dimensional material [14]. Single graphene sheets can be stacked on each other, forming graphite which has a weak van der Waals bond between layers [15]. Graphene was one of the first two-dimensional materials produced and can be shaped into different forms with different dimensionalities [14]. Diagram 3 helps visualize graphene on a microstructure level.

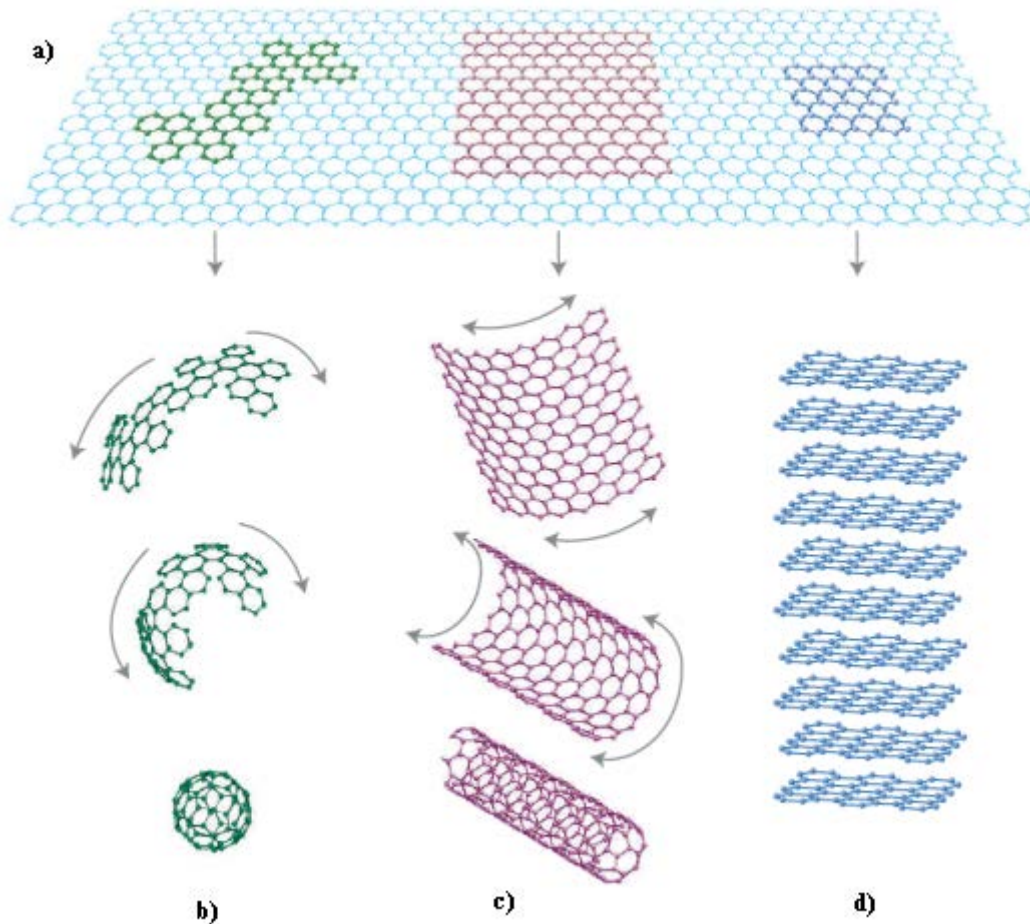


**Figure 3.** Some of the different forms graphene can take: a) single sheet of graphene b) buckyballs, c) nanotube, d) graphite. Taken from reference 14.

Graphene offers a very high theoretical surface area [3]. Single-layer graphene was calculated to have a surface area of  $2630 \text{ m}^2/\text{g}$  [3]. To put that in perspective, a high surface area material is considered to have a surface area anywhere from  $300 \text{ m}^2/\text{g}$  to  $2000 \text{ m}^2/\text{g}$  [16]. This makes it an excellent choice for use as an ultracapacitor material. Graphene is also suitable for different kinds of electrodes [3] and has a very high intrinsic, in-plane electrical conductivity along with high mechanical strength and chemical stability [5]. These properties allow graphene to achieve one of the highest energy densities of any known ultracapacitor material— $136 \text{ Wh/kg}$  at  $80 \text{ }^\circ\text{C}$  [17]. This is comparable to a nickel metal hydride battery.

However, there is a way to improve the conductivity of graphene. Chemical doping of carbon materials can increase its electrical conductivity and free charge-carrier densities [18]. By doping a graphene lattice with nitrogen it acquires properties similar to an *n-type* semiconductor.

Semiconductors provide an intermediate level of electric conductivity as compared to metals which have high conductivity and insulators which have low conductivity [19]. Due to the lower conductivity, semiconductors require a sufficient amount of energy to allow for electron motion. A method of improving a semiconductor's conductivity is to induce impurities into the semiconductor material—a method known as doping [19].

Introducing impurities into a semiconductor material can create one of two types of semiconductors: *p-type* or *n-type* [19]. A *p-type* impurity is known as an acceptor atom. Acceptor atoms create “holes” in the semiconductor by taking away (accepting) weakly bound outer electrons from the semiconductor material. *N-type* impurities, on the other hand, are known as donor atoms because they provide extra electrons to the host material. These extra electrons act as charge carrier, moving relatively freely inside a lattice structure, thereby increasing conductivity. Nitrogen is a natural choice for an impurity among the list of potential dopants [18]. Carbon is a group IV solid (group IV elements contain four valence electrons). To create *n-type* semiconductors, group V elements are commonly used as impurities to group IV elements [19]. This is because group V elements contain five loosely bound valence electrons, easily allowing it to donate an electron to the host material [19]. Not only is nitrogen is a group V element, but it is the group V element closest in size to a carbon atom, allowing it to more easily fit into a graphene lattice [20].

It should be noted that pristine graphene has no semiconducting gap; however other researchers have confirmed that a bandgap is created in graphene when it is doped with nitrogen atoms [20]. Nitrogen also increases graphene's density of electronic states at the Fermi level [18].

### **C. THESIS OBJECTIVE**

There are several objectives for this research:

- Develop protocols for the synthesis of nitrogen doped graphene; more importantly, mechanisms for controlling the amount of nitrogen in the graphene lattice.
- Test the usefulness of using a reduction-expansion method, aided by urea, to promote doping graphene.
- Experiment with microwave plasma methods as an alternative to produce nitrogen doped graphene.
- Fully characterize the structure, microstructure, surface area and nitrogen content of the product materials, doped and undoped.
- Determine which technique will provide a reliable path to determine the amounts of nitrogen introduced into the graphene lattice.

### **D. HYPOTHESIS**

The methods used in this research to generate graphene will produce samples with controlled levels of nitrogen.

THIS PAGE INTENTIONALLY LEFT BLANK

## II. EXPERIMENTAL METHODS

### A. GRAPHENE PRODUCTION BACKGROUND

Graphene is essentially ten or fewer sheets of graphite. In a sense, producing graphene is not difficult at all—in fact it’s done incidentally all the time. For example, when writing with a pencil, small graphene sheets are created [21]. Producing graphene with desirable attributes, however, is very difficult. There are many methods to produce graphene. The most common ones are discussed in the following paragraphs.

One of the best-known methods of producing graphene (and one that has led to many different research efforts on the material) is the drawing method. It is also known as the “scotch tape” method because of how the earliest form this method was conducted. Originally, researchers took graphite and gradually reduced it to thinner and thinner pieces using an adhesive tape [14]. This tape (now containing pieces of graphene) was dissolved in a solution and placed on silicon. These pieces were small and could only be viewed under a microscope [22]. This method was quickly refined and increasingly larger graphene flakes were produced. A slightly different form of the method involves pushing bulk graphite along a silicon surface to produce graphene sheets. In either case, silicon (coated with a thin film of silicon oxide) was chosen as the preferred surface because it provides enough optical contrast with graphene for the human eye to detect with the aid of an optical microscope [22]. However, having the right thickness for the silicon oxide coating (typically 300 nm) is very important. Deviating from this thickness, even slightly, causes the graphene to become indistinguishable from the background [14].

Researchers at the University of Bristol produced graphene by a method known as chemical vapor deposition (CVD) [23]. Inside a quartz tube furnace heated to over 1000° C, they grew graphene on a copper foil in an atmosphere of methane and hydrogen. The CVD method is able to create large graphene films and (as an advantage over the epitaxial growth method) graphene growth automatically stops after one graphene layer is created (at least when using copper) [24]. Researchers believe that one of the reasons for this self-limiting behavior is because carbon has a low solubility in copper. One

interesting variant to this method was discovered by researchers at Rice University. Chemists there used sucrose as the base substance for graphene growth [25]. They speculate that it could be scaled up for industrial uses.

Somewhat similar to the chemical vapor deposition method described earlier is the epitaxial growth method. This method involves taking an element that has been infused or bonded with carbon and then “growing” sheets of graphene on its surface. One of the most common materials researchers are using for this method is silicon carbide. To grow graphene on silicon carbide researchers heated graphene to temperatures in excess of 1100° Celsius [26]. When this heating process is done in a noble gas atmosphere, it causes the silicon to sublime. This leaves large layers of graphene on the surface. Interestingly, certain properties of the graphene that is produced (such as thickness or electrical properties) are determined by the size of the silicon carbide used to grow the graphene [26].

Besides silicon, certain metals have also been used for the epitaxial growth of graphene. Ruthenium is one such metal [27]. To grow graphene on ruthenium, researchers first took the metal and heated it to 1150° C. This caused the ruthenium sample to absorb carbon atoms. The sample was subsequently cooled to 850° C. The carbon that had been absorbed rose to the surface—initially as isolated single-layer structures (about 100 micrometers in diameter). After this the graphene consolidated to cover about 80% of the sample surface. At this point, additional layers of graphene grew. A disadvantage of using ruthenium is that the first graphene layer has a strong interaction with the ruthenium sample (although the subsequent layers do not experience this issue). The thickness in the graphene layers is not uniform either. When iridium is used in place of ruthenium, it seems to avoid these problems [28]. The graphene produced is of uniform thickness, highly ordered and is has a weak bond with iridium. Unfortunately, both ruthenium and iridium are both very expensive.

Another method—and perhaps the oldest way to produce graphene—is graphitic oxide reduction. This method was first developed by a German scientist of the name H. P. Boehm [29]. Although there are different variants of this method, the basic idea is that graphitic oxide is heated rapidly to exfoliate it and thus produces a much dispersed form

of carbon that contains graphene flakes [10]. This is the most promising method for creating graphene for ultracapacitor electrodes because it produces “substrate free” or “self-standing” graphene. Self-standing graphene can be scaled up with relative ease and little cost.

That is why the rapid exfoliation of graphitic oxide was chosen for this study. The addition of urea (which, among other things, acts as a reduction-expansion agent) is a variation of this process that is described in subsequent sections of this paper.

There are advantages to using urea with this method [30]. The precursor materials are, in addition to being non-toxic and environmentally benign, inexpensive. Less energy is required to produce graphene when compared to other thermal methods (urea, when vaporized, causes mechanical expansion of graphitic oxide). Also, fewer oxygen groups remain in the graphene. When using urea as a reduction-expansion agent the leftover oxygen in the graphene lattice drops to below 3% as opposed to more than 8% without using urea [30]. Also, according to the hypothesis, by controlling the quantity of urea used the amount of nitrogen in the graphene can be adjusted.

## **B. PRODUCTION OF GRAPHITIC OXIDE**

In order to produce graphitic oxide (GO) we used a variation of the improved Hummer’s method first developed by a research group at Rice University [31]. Sigma Aldrich Graphite Powder (<20  $\mu\text{m}$ , synthetic) was used as the graphite base material. A mixture of  $\text{H}_2\text{SO}_4/\text{H}_3\text{PO}_4$  (150:16 mL) was combined with 1.25 g of graphite powder and 7.5 grams of  $\text{KMnO}_4$ . The solution was then maintained at a maximum temperature of 40° C and stirred for 8 hours in a magnetic mixer. After cooling to room temperature, 20 mL of de-ionized ice was added. Then 1.5 mL of  $\text{H}_2\text{O}_2$  was added, which caused solution to change to a brown-green color. The solution was then placed in centrifuge tubes and processed for 4 minutes at 4000 rpm. The supernatant was drained, leaving a solid material in the sample holder. De-ionized water was added to the solid, shaken by hand, then returned to the centrifuge configured for the same settings as before. This step was then repeated, however a 30% solution of HCl was used in place of water. Next, this step was repeated one more time using ethanol. After sample was drained for the final

time, the subsequent mixture was poured onto a ceramic disk and dried in an oven at 40° C for 60 minutes. The remaining solid material was allowed to cool to room temperature before being collected.

### **C. PRODUCTION OF NITROGEN-DOPED GRAPHENE**

To produce graphene from graphitic oxide, two methods were used. One method was first proposed by our group [30]. It involved heating a precursor mixture of GO and urea in a quartz tube with gas flowing past the samples in a furnace. A major difference between this effort and earlier studies is that diverse GO:urea ratios were used in order to control nitrogen amounts.

The second method used an approach known as the aerosol-through-plasma (ATP) method. Producing graphene by means of ATP was first successfully performed directly from hydrocarbons as described by other researchers [32], although the process had extremely low yields. Afterwards, another research team produced ATP graphene from GO [33]. The procedure described in the later paper is very similar to what was performed for this research. Essentially, a crushed GO precursor is mixed with different gasses to produce an aerosol and subsequently passed through plasma. The resultant product is graphene. The research for this paper varied the process by adding nitrogen gas to the aerosol.

Each process is explained in greater detail:

#### **1. Method 1: Expansion-Reduction**

Varying quantities of GO, along with urea, were crushed in a mortar. The ratio of urea to GO was varied in order to obtain different levels of nitrogen in each resulting graphene sample. Each sample had a different urea ratio based on an overall quantity of five parts GO. Table 1 contains weights of each amount of GO and urea used for each sample along with the resulting weight of the graphene. In all cases, approximately 0.1 grams of GO were used.

After the GO and urea mixture was prepared it was placed in a ceramic boat and moved into a quartz tube. One end of the tube was connected to a tank of nitrogen gas

and the other end was connected to a ventilation hood. Nitrogen gas was passed through the tube at a rate of 364.1 sccm for 20 minutes. The purpose of this was to purge oxygen from the tube.

After 20 minutes, nitrogen flow was reduced to 13.9 sccm and tube was placed into furnace that was preheated to 600° C. Tube remained in furnace for 10 minutes then was removed and allowed to cool to room temperature (approximately 30 minutes). Gas flow was closed and quartz tube was removed from its connections. The ceramic boat was removed from the tube and sample was collected, weighed and placed in a sample holder which was labeled.

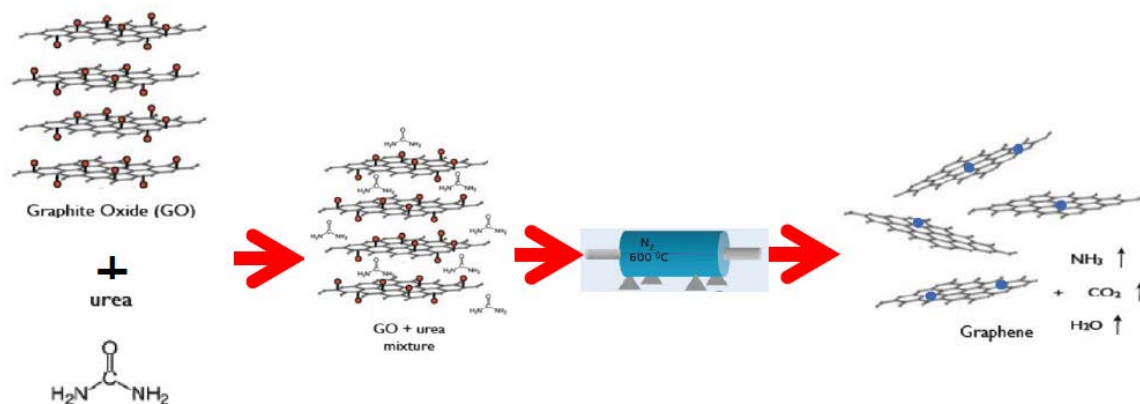


**Figure 4.** Overall process of the expansion-reduction method. GO and urea are crushed together in a mortar to form a GO+urea mixture. The mixture is then rapidly heated in a furnace under an inert gas. The result is self-standing graphene sheets where most of the oxygen groups have been removed and (we believe) nitrogen inserted into the lattice.

GO/Urea Ratio (R)	Quantity of GO (grams)	Quantity of Urea (grams)	Quantity of Graphene Produced (grams)
5	0.1031	0.0201	0.0224
4	~0.1000	~0.0250	
2.5	0.1002	0.0402	0.0304
1.6	0.1005	0.0610	0.0252
1.25	0.1004	0.0798	0.0164
1	0.0999	0.1005	0.0315
0.3	~0.1000	~0.3333	0.0487

**Table 1.** Shows the approximate weights of GO and urea used to prepare each sample and the result weight of the product.



**Figure 5.** Picture of furnace with quartz tube.

## **2. Method 2: Aerosol-Through-Plasma (ATP)**

The ATP method generates a microwave plasma discharge by means of a magnetron and argon gas. The precursors of interest, that is, the solid to be reacted, is placed in a beaker where it mixes with a gas to form an aerosol, which travels through an alumina tube directed to the hot zone. There, the precursor encounters high temperatures (in the order of 2,000-3,000° C, depending on the gases used) and transforms (vaporizes, reacts). Farther along the line, the species formed solidify as the mixture travels through the chimney and cools down. The products are subsequently collected in a filter (see figure 6).

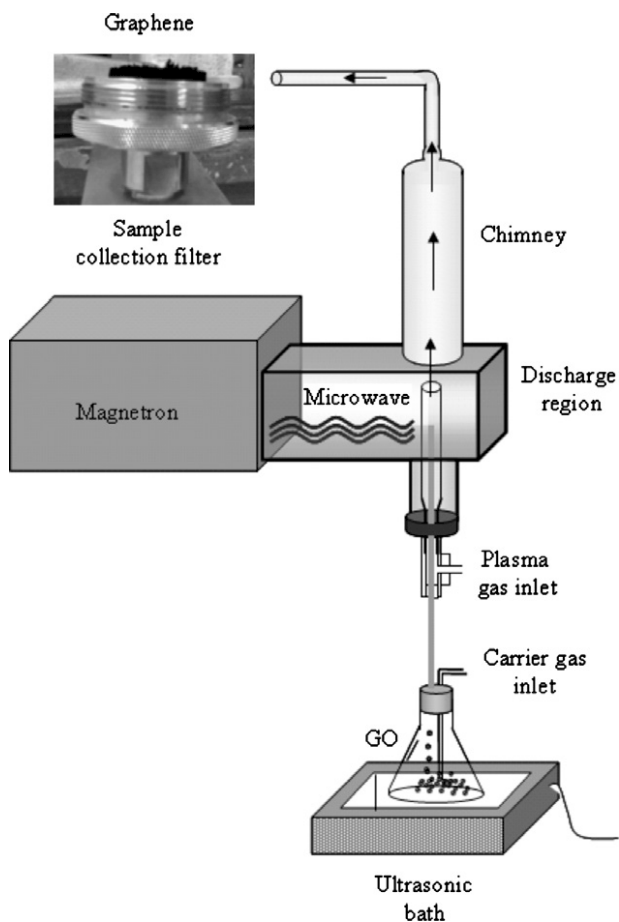


**Figure 6.** Schematic of the microwave atmospheric torch system used to produce graphene from GO. Taken from reference 33.

No urea was used for samples ran through the plasma device. Instead, nitrogen was added to the GO by means of passing it through a gas. This method was used twice. The first time the sample was passed through device using argon gas only. The second time used both argon and nitrogen gas. The procedure for each sample run was nearly identical with minor parameter changes. Those parameter changes are noted below. Also included below is a chart containing the weights of the initial GO used for each sample and the weight of the resulting graphene that was produced.

GO was crushed in a mortar. The plasma device was started and set at the following parameters: 900 forward watts and 002 reflected watts. The crushed GO was placed in a beaker that was then connected to an intake tube. The bottom of the beaker rested in a shallow water level which was vibrated to serve as an ultrasonic bath. This

caused the GO to incrementally jump and mix with a carrier gas (in this case argon, which was set at a 3650 sccm flow rate). This new aerosol mixture traveled through an alumina tube to a plasma discharge zone. The GO reacted to the hot zone as it passed through it. The transformed GO moved to an afterglow region in a chimney connected to a filter system. The filter collected the particles as they deposit on its surface (a vacuum pump controls the pressure of the system to help ensure a negative pressure, although the pressure values are in all cases very close to atmospheric conditions). For this particular run, the argon flow rate was increased to 4410 sccm after 18 minutes to improve GO flow rate. At 19 minutes, the argon flow was stopped. After ensuring that no more sample material was flowing, the machine was shutdown (allowing for a 15 minute cooldown time during shutdown procedure). Afterward, the filter was removed and the product was collected.

For the second run, a flow of nitrogen gas was introduced into the aerosol stream. The procedure for this run is the same as described above with exceptions listed as follows. Argon flow rate was set to 3650 sccm and nitrogen flow rate at 1529.9 sccm. Start parameters were 900 forward watts and 003-005 reflected watts. Flow rate for both gasses remained unchanged throughout run, however reflected watts crept upward requiring adjustments on smart meter to bring it down.

Gas	Quantity of GO (grams)	Quantity of Graphene Produced (mg)
Argon	0.0389	5
Argon and Nitrogen	0.2578	15

**Table 2.** Shows the weight of the GO precursor used and the weight of the product.

THIS PAGE INTENTIONALLY LEFT BLANK

### III. CHARACTERIZATION

#### A. X-RAY DIFFRACTION

##### 1. Purpose

X-Ray Diffraction (XRD) analysis was performed on all samples in order to help determine the crystallinity and verify the existence of the various species and carbon phases. XRD does not directly measure what elements may be in a given material, rather it identifies crystal phases, orientations and dimensions. XRD identifies the crystal structure of a sample which is in turn dependent on what types of elements are present and how they are bonded to each other to form a solid with long range order. It does this by producing an X-ray beam. The XRD creates X-rays by using two metal electrodes (an anode and cathode). The cathode, when heated, emits electron that accelerate toward the anode. When the electrons hit the anode, both heat and X-rays are emitted (the anode is cooled with a chilled water system). Only 1% of the electron energy actually produces X-rays. When an electron collides with another electron in the inner shell of an anode atom it may eject that electron. If this happens, an electron from the outer shell must move to the inner shell. Electrons move between shells is what produces the X-rays [34].

The X-ray beam is shot at a sample material and interacts with the different set of crystalline planes present. This interaction produces a diffraction pattern. The scattering is governed by Bragg's Law:  $n\lambda=2d\sin\theta$ , where  $n$  (an integer) and  $\lambda$  (wavelength of the X-ray beam) are determined by the design of the XRD analyzer. The Bragg angle ( $\theta$ ) is the angle between the source of the incident wave and the scattering planes. Two times the Bragg angle ( $2\theta$ ) is the angle between the incident wave source and scattering wave detector. An XRD analyzer controls the  $2\theta$  variable while recording the intensity or "counts" produced from the scattering at each particular angle. The counts will vary as a function of  $d$  (the lattice spacing between the crystalline planes) [34].

What is of interest in this study is how the peak intensity shifts in position along the  $2\theta$  axis per sample. A shift to the right indicates that the  $d$  spacing is decreasing, thus there is less space between the different graphene layers. Decreasing space between

layers would be consistent with the hypothesis that more nitrogen has been inserted into the graphene lattice. Nitrogen, because it is donating extra valence electrons, causes the graphene sheets to become more attracted to one another and compress the overall sample.

## 2. Testing Parameters

The XRD analyzer used at NPS is the Phillips PW1830 Diffractometer (shown in figure 7). It is composed of three principle parts: the X-ray source, the goniometer (which holds the sample) and the X-ray detector. The source (where the X-rays are actually created) is an X-ray tube. This tube is, essentially, a vacuum chamber that contains the anode and cathode.



**Figure 7. Photograph of a Phillips PW1830 Diffractometer.**

The Phillips PW1830 Diffractometer uses a tungsten filament as its cathode and copper for its anode. It creates electromagnetic radiation with energies anywhere from 200 eV to 1 MeV. The anode produces  $\text{Cu K}_\alpha$  X-ray radiation with an energy of 8.04

KeV. The X-rays have a wavelength of 1.5418 Å. All samples were prepared by pressing powder onto a silicon disc sample holder (no bonding agent was required). The settings for all analyses were as follows:  $2\theta$  was measured from  $5^\circ$  to  $70^\circ$  in step increments of  $0.025^\circ$ . Diffractometer was set at a voltage of 35 kV and a current of 30 mA. All analyses were conducted in accordance with NPS standard operating procedures.

## **B. BET ANALYSIS**

### **1. Purpose**

BET is an acronym consisting of the first letter of the surnames from the three scientists who developed the analysis theory: Stephen Brunauer, Paul Hugh Emmett and Edward Teller [35]. BET analysis measures the surface area of nano particles. As described earlier, a high surface area is a desirable characteristic of ultracapacitor electrodes. A BET surface analysis was conducted on all prepared samples.

BET analysis essential measures surface area of nanoparticles by quantifying the amount of gas that is adsorbed to their surface [36]. When a gas atom or molecule binds to the surface a material (but is not absorbed into the material) that is called adsorption. The BET theory allows researchers to estimate how many gas molecules are required to create an adsorbent layer on the surface of a nanoparticle. Surface area can then be calculated by multiplying that number with the cross-sectional area of an adsorbate molecule [37].

How much gas is adsorbed to a material's surface depends on many factors, such as the characteristics of both the gas and material, temperature and pressure. Because it has a strong interaction with most solids, nitrogen gas is typically used in this process. Even then, however, the interaction is still weak, so samples are usually cooled with liquid nitrogen in order to force more gas to adsorb to the particles. With a sufficiently cooled sample, nitrogen gas fills the sample chamber. The amount of gas is released in measured increments. The sample chamber remains under a partial vacuum in order to achieve the saturation pressure (the lowest pressure at which the maximum amount of adsorption occurs). Sensors (pressure transducers) detect any small changes in pressure

due to the creation of adsorption layers. Once the layers are formed, unadsorbed nitrogen gas is removed from the sample chamber and the sample is heated to release all the gas that was adsorbed. The amount of gas released is measured and plotted on an isotherm. The sample is then weighed. Any change in weight due to the process is used as a correction factor.

## **2. Testing Parameters**

In order to conduct a BET analysis at the Naval Postgraduate School, we used the NOVA 4200e Series Surface Area and Pore Size Analyzer (see figure 8). The surface analyzer consists of two compartments. One compartment is devoted to degassing the sample chambers. It is critical that a sample is degassed prior to the surface analysis to help remove water and possible absorbed molecules [37]. The degassing compartment is configured and connected to a vacuum pump. Heating mantles (in which the sample chambers can be sheathed) are used to heat the sample (to an adjustable temperature) while being degassed. The other compartment is where the actual analysis process occurs. The compartment has flow lines leading to both a vacuum pump and a nitrogen tank (configuration is adjustable and occurs automatically as part of the process). The compartment also contains a stage to hold a cylinder of liquid nitrogen used to cool the sample. The stage is able to rise and lower automatically. Programming is done through a nearby computer and a display panel on the device. All data is collected on the computer.

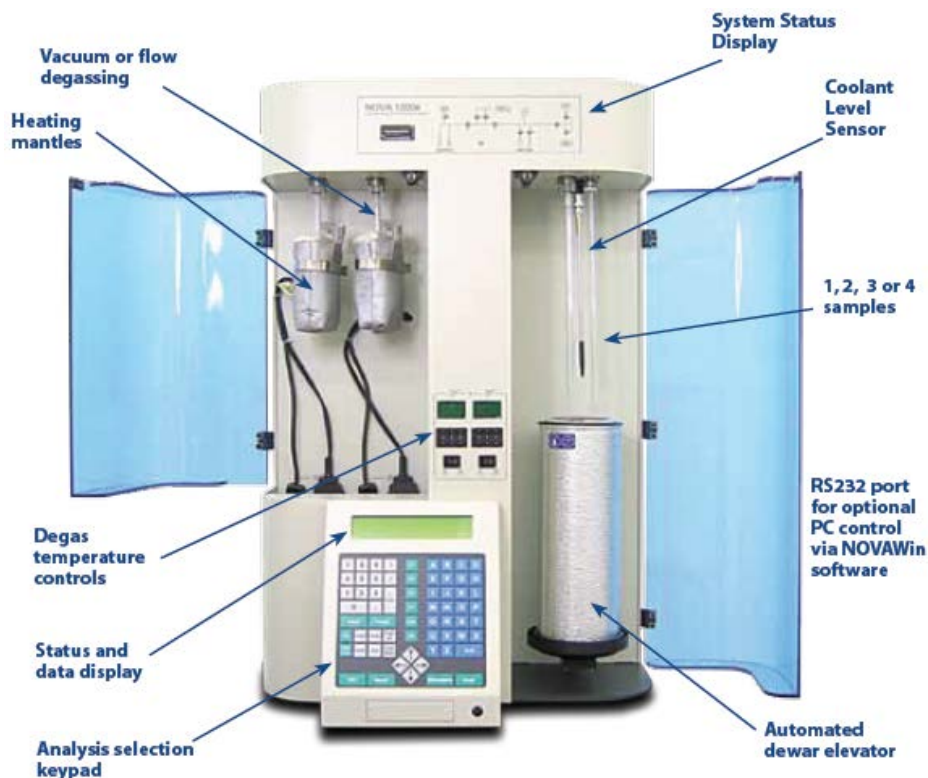


Figure 8. Diagram of a NOVAe Series Surface Area Analyzer. Taken from reference 37.

Samples were prepared by placing them in separate glass bulb chambers and glass rods were inserted into the chambers (previously calibrated). The chambers were then placed in the degassing compartment and heating mantles were attached. Samples were then degassed for 10 minutes at room temperature. Next, the samples (still being degassed) were heated to 100° C for 30 minutes. Then temperature was then increased to 300° C for 150 minutes (TGA experiments determined the samples remained stable up to 450° C). After degassing was complete, the heating mantles were removed and the chambers were permitted to cool to room temperature under nitrogen. Once at room temperature, samples were then placed in the analysis compartment. A dewar of liquid nitrogen was placed underneath the samples to cool them. A pre-programmed configuration controlled when and how the stage was raised as well as how nitrogen was inserted into the chamber. After the adsorption phase was complete, the chamber was vacuumed and the amount of nitrogen released was recorded as the samples returned to room temperature. Afterward, the samples were removed from chambers and weighed.

Weights were entered into the computer as a correction factor and surface area data was collected.

## **C. RAMAN SPECTROSCOPY**

### **1. Purpose**

Raman spectroscopy is a vibrational spectroscopy technique that utilizes the so-called Raman Effect. The Raman Effect was first discovered by Chandrasekhara Venkata Raman in 1921 [38]. The Raman Effect describes changes that light might undergo after it interacts with a material. When photons from a light source make contact with a material they are absorbed, then reemitted. If the reemitted photons have the same frequency as the source photons, those photons have gone through elastic scattering [39]. Elastic scattering is also known as Rayleigh scattering [39]. However, a fraction of the reemitted photons have a different frequency than the source photons. These photons have undergone inelastic scattering, referred to as Raman scattering [39]. Only a small fraction of source photons (approximately 1 in 10 million) undergoes Raman scattering [39].

Researchers further distinguish between Stokes and anti-Stokes Raman scattering. Stokes is the most common form of scattering at ambient conditions [40]. In Stokes scattering, a source photon interacts with a molecule that is at a basic (non-excited) vibrational state and loses energy to that molecule. The resulting emitted photon has a lower energy state. In anti-Stokes scattering, the opposite occurs. Source photons interact with molecules in an excited vibrational state and gain energy from the molecule. Emitted photons have a higher energy state [39]. These changes in energy states or frequencies (Raman shifts) can be very large, up to tens of thousands of wavenumbers. The magnitude of these shifts is determined exclusively by the material and the vibrational mode involved [40].

### **2. Testing Parameters**

The Raman spectroscopy was performed using a Renishaw inVia Raman Microspectrometer with a 514 nm laser excitation. Measurements were taken under a 1800 l/mm grating and with a notch filter. The following parameters were set: 20x

magnification long focus objective lens, 10% laser power, 10 accumulations with a 20 sec exposure time per accumulation. Scans were centered at 1500 Raman shifts/cm. Cosmic ray removal was selected to remove abnormal data spikes as the result of background noise. To further reduce background interference, all lights in the immediate vicinity were either turned off or were covered. All readings were performed at room temperature.



**Figure 9. Photograph of a Renishaw inVia Raman Microscope.**

Specimens were prepared by placing small quantities of a sample on a quartz slide with a spatula (no bonding agent was required). The slide was then placed on stage where it was optically focused using manual knobs. Scans were then executed using the measurement parameters listed earlier.

## **D. SCANNING ELECTRON MICROSCOPE**

### **1. Purpose**

Scanning Electron Microscopy (SEM) is an analytical technique that produces high-magnification images. An SEM accomplishes this by shooting a beam of high-energy electrons at a sample material [41]. Electrons are created by heating a cathode filament. These source electrons can collide with the sample in one of two ways [42]. If the electrons collide with a nucleus, they undergo an elastic collision which produces backscattered electrons. If the source electrons collide with the sample electrons then

they undergo an inelastic collision. Inelastic collisions result in many different types of radiation. Secondary electrons (electrons emitted from the sample) are the type of radiation used to generate SEM images [41]. Secondary electrons are monitored with a secondary electron detector. Software converts the data from the secondary electron detector into an image.

An SEM can achieve much greater magnification compared to an optical microscope that uses light. The maximum magnification that a light microscope can achieve is approximately 2,000x, but an electron microscope can achieve 75,000 or even greater [42]. This is because the wavelength of optical light (390-750 nm) is much larger than the wavelength of the source electrons (0.05 nm) [42]. Under diffraction, the difference in wavelength allows for a higher resolution using Bragg's Law. However, SEMs do require that scans be conducted in a vacuum. A vacuum removes gas molecules in the chamber which may scatter the electron beam. The absence of gas molecules also reduces oxidation of the cathode filament.

## **2. Testing Parameters**

SEM was conducted with a Zeiss NEON 40 field emission SEM with focused ion beam. Images were taken with the "InLens" setting at 20kV. Working distance for all images was approximately 4.6 mm. Four images of each sample were taken. Each images was of at a different magnification (15,000x, 20,000x, 40,000x and 60,000x).

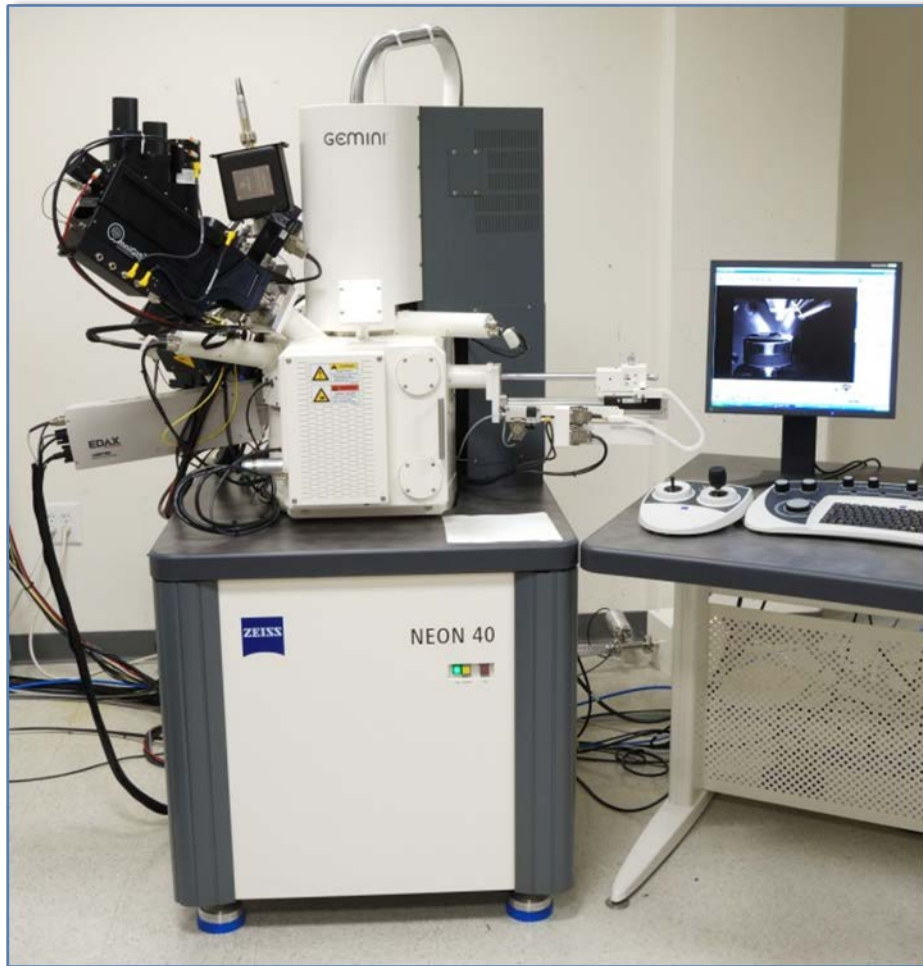


**Figure 10.** Photograph of a Zeiss NEON 40 field emission SEM Microscope.

Specimens were prepared by double-sided carbon tape on sample mounts. A tiny amount of sample was placed on top of the carbon tape and flattened with a spatula. The mounts were placed in a specimen case which was in turn placed in a vacuum chamber overnight. Afterward, the specimen case was removed and the sample mounts were placed and tightened on a mount platform. The platform was then attached to the SEM stage. Once the stage door was closed, the SEM chamber was vacuumed. Once the vacuum was complete, the scans were conducted. Following the scans, the chamber was restored to room pressure and sample mounts were removed from the platform and returned to specimen case. The SEM chamber was placed back into a vacuum. All scans were conducted in accordance with NPS standard operating procedures.

## **E. THERMOGRAVIMETRIC ANALYSIS**

### **1. Purpose**

Thermogravimetric Analysis (TGA) is a process where the mass of a sample is measured as it is heated to a specific temperature at a specific rate in an inert (or reactive) atmosphere [43]. A sample is placed in a holder or pan that is, in turn, placed on a mass balance shield inside of a furnace. The furnace is controlled by a thermocouple attached to the sample holder. The balance itself is separated from the furnace so the temperature changes do not affect it. Prior to heating the sample, a purge gas creates a specific environment inside the furnace [43]. The gas continues to flow during heating and leaves through an exhaust terminal (in this case, it leads to a mass spectrometer which will be described in the following section). Results are displayed in a graph that can either plot mass change as a function of time or of temperature.

The plot is useful for quantifying oxidation, reduction, decomposition, loss of water, loss of a solvent and more [43]. Comparing plots of graphene samples prepared without urea versus those with urea can provide clues as to whether nitrogen is being inserted into a graphene lattice.

### **2. Testing Parameters**

The TGA of samples was conducted on a NETZSCH STA 449 F3 Jupiter Thermal Analyzer. Argon gas was used as the atmospheric gas for all experiments that tested sample reactivity. The start temperature was at room temperature and the end temperature was 900° C. The heating rate was 5° C/min. The protective gas flow was 20 mL/min and the purge gas flow was 20 mL/min.



**Figure 11. Photograph of the NETZSCH STA 449 F3 Jupiter Thermal Analyzer.**

A small, pre-weighed portion of a sample was placed on a sample stand inside the furnace. After the sample was loaded into the TGA, the device was closed and air was removed from inside the furnace using an attached vacuum pump. When the vacuum reached 97%, the furnace was filled with argon gas. Once the chamber was filled, it was again vacuumed to 97% then re-filled with argon gas. This process was performed for a total of three times to remove all residual atmospheric gases. After the furnace was filled with argon gas for the last time, pre-programmed software carried out the experiment under the conditions described earlier. The software also performed all data processing.

The samples were also studied by this technique under  $O_2$  containing atmospheres. The process is known as Temperature Programmed Oxidation (TPO). In such, the carbon based solid transforms, at high temperatures, into  $CO_2$  while nitrogen contained in sample turns into  $NO_2$ . Nitrogen doped graphene will burn off at temperatures above  $550^\circ C$  to render only  $CO_2$  and  $NO_2$  with no solid byproducts. All BET experiments were conducted in accordance with NPS standard operating procedures.

## **F. MASS SPECTROMETRY**

### **1. Purpose**

Mass spectrometry is an analysis technique that deflects or separates charged gas ions by their mass. This ultimately helps researchers determine a sample's component structure, component concentrations and isotopic composition [44]. While there are many different kinds of mass spectrometry methods, all share the following: an inlet system for the sample, an ionization process, an ion accelerator, an ion separating process and an identification system [44]. By analyzing the evolved gases from the samples, it is possible to determine if nitrogen groups are present. This would suggest that adding urea to GO can lead to graphene sheets with nitrogen in the lattice structure.

The particular type of mass spectrometry analyzer used in this study is known as the quadrupole mass analyzer. Quadrupoles, like all mass analyzers, separate ions according to their mass-to-charge ratios. The speed with which ions travel is inversely correlated with their mass (the fastest ions have the smallest mass and the slowest ions have the largest mass) [44]. This type of analyzer consists of four metal electrodes shaped like rods (thus the reason for the term 'quadrupole'). In this device, gas molecules are ionized then accelerated through an electromagnetic field. After this they must pass through a space between the four rods and then onto an ion detector (see figure 12). Each rod is electrically coupled to the one across from it with a dc potential applied to each pair along with a low amplitude-high frequency ac potential (see figure 13) [44]. This causes one set of rods to act as anodes and the other set as cathodes. If an ion is attracted to one of the electrodes and makes contact with it, it becomes grounded and fails to travel to the ion detector. Effectively, this makes the space between the rods a narrow-pass filter for the ions [44]. The dc and ac potentials can be adjusted in such a way that ions with a small mass-to-charge ratio can first pass through followed by ions of ever increasing mass-to-charge ratios [44].

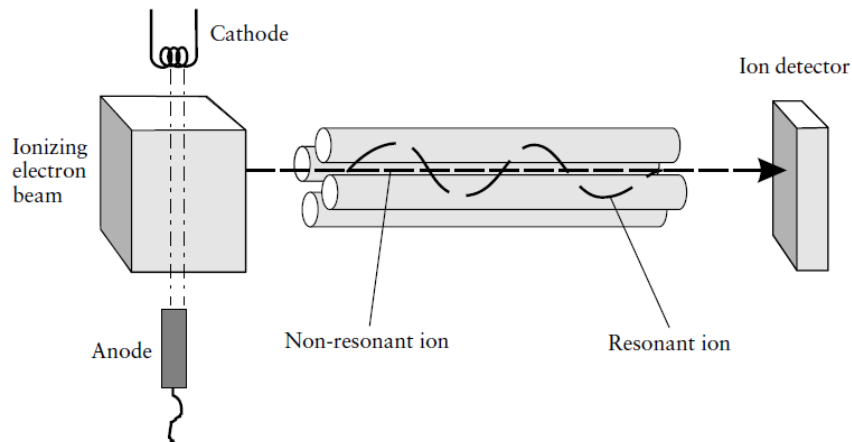


**Figure 12.** Diagram of a basic quadrupole mass analyzer configuration. Taken from reference 44.

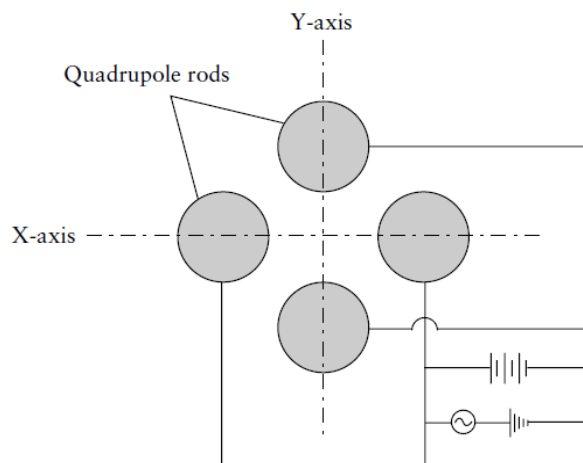


**Figure 13.** Diagram showing how rods are electrically connected inside a quadrupole mass analyzer. Taken from reference 44.

## 2. Testing Parameters

Mass spectrometry was performed simultaneously with the thermogravimetric analysis. The testing of samples was conducted on a NETZSCH QMS 403 C *Aëolos* Quadrupole Mass Spectrometer that was linked to thermal analyzer (see figure 14). Evolved gasses produced from TGA were passed through the mass spectrometer, analyzed and recorded on the system's software. Condensation was avoided because the transfer system was heated and there were no pressure reduction orifices [45]. The QMS 403 C *Aëolos* Quadrupole Mass Spectrometer uses a 2 Y<sub>2</sub>O<sub>3</sub>-coated iridium cathode and a

Faraday and SEV (Channeltron) detector [45]. It uses an electron impact ion source at 100 eV [45].

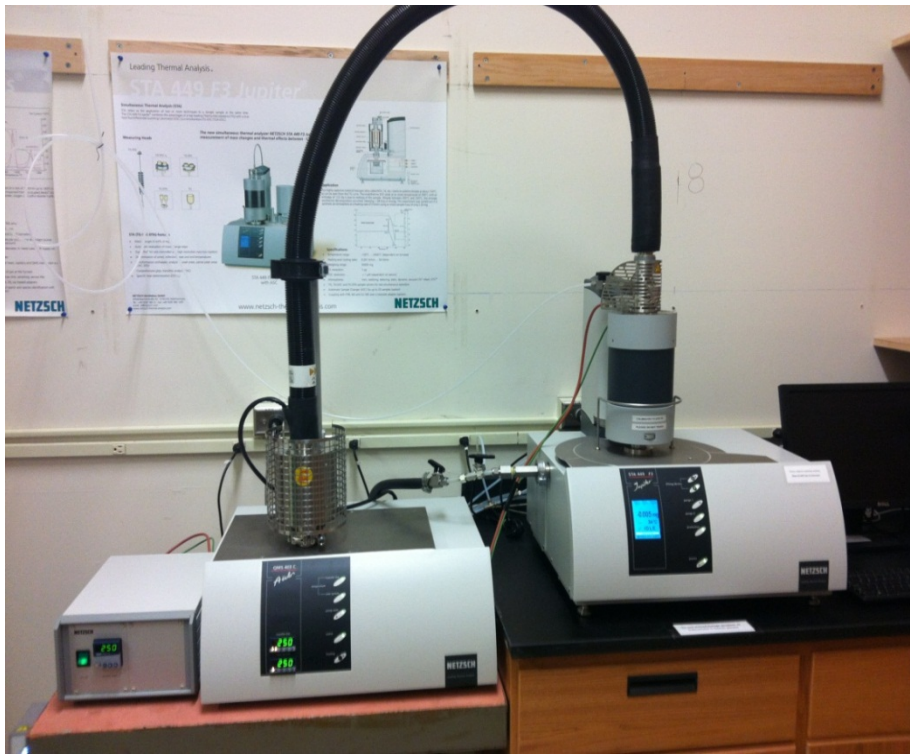


**Figure 14.** Photograph of the NETZSCH QMS 403 C *Aëolos* Quadrupole Mass Spectrometer (device on the left connection) linked to the NETZSCH STA 449 F3 Jupiter Thermal Analyzer (device on the right connection).

THIS PAGE INTENTIONALLY LEFT BLANK

## IV. RESULTS AND DISCUSSION

### A. X-RAY DIFFRACTION

To serve as a baseline comparison, a test was conducted with an empty slide to show what background noise is produced simply from the silicon:

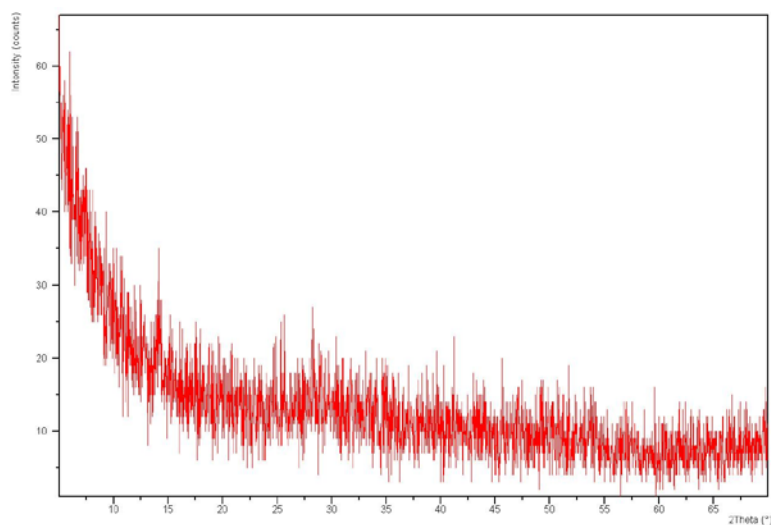


Figure 15. XRD results from analysis with an empty sample disc.

A sample of unaltered GO was also analyzed (see figure 16). There is a prominent spike in intensity at roughly  $2\theta=8^\circ$  with a smaller peak near  $2\theta=43^\circ$ .

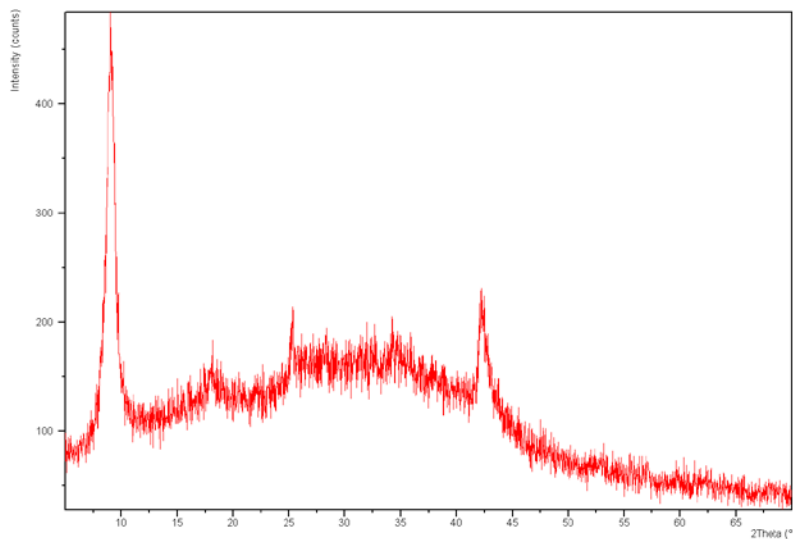
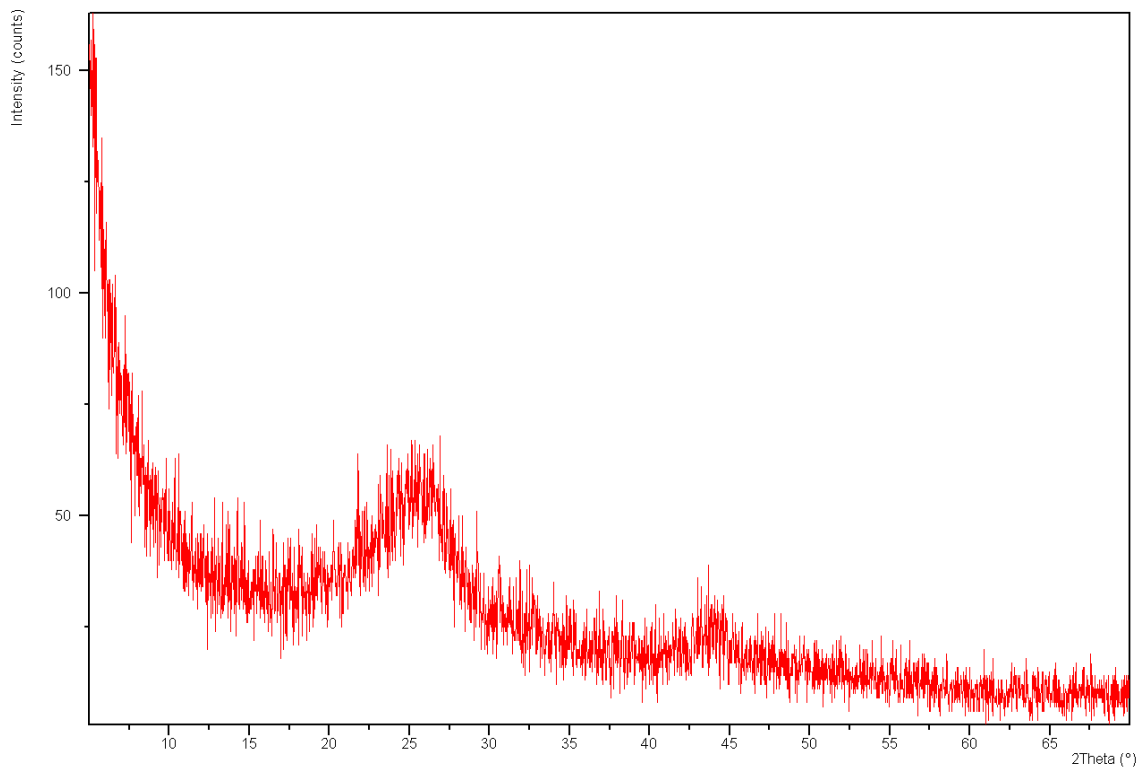


Figure 16. XRD results from analysis of unaltered GO.

A graphene sample prepared with the expansion-reduction method (without the addition of urea) is shown here:



**Figure 17. XRD results from analysis of thermally expanded GO without urea.**

The peak that originally appears at  $2\theta=8^\circ$  is now gone. Instead, a new peak has appeared at  $26^\circ$ . This peak is associated with the (002) Miller index plane of graphite. The secondary peak has from the GO sample shifted to the right somewhat. These changes are consistent with what other researchers have found and show that the GO is, in fact, being converted to graphene <sup>[30]</sup>.

Every graphene sample prepared with the expansion-reduction method (with varying levels of urea added) was also analyzed. Figure 18 overlays all these results with the simple thermally expanded GO and unaltered GO results:

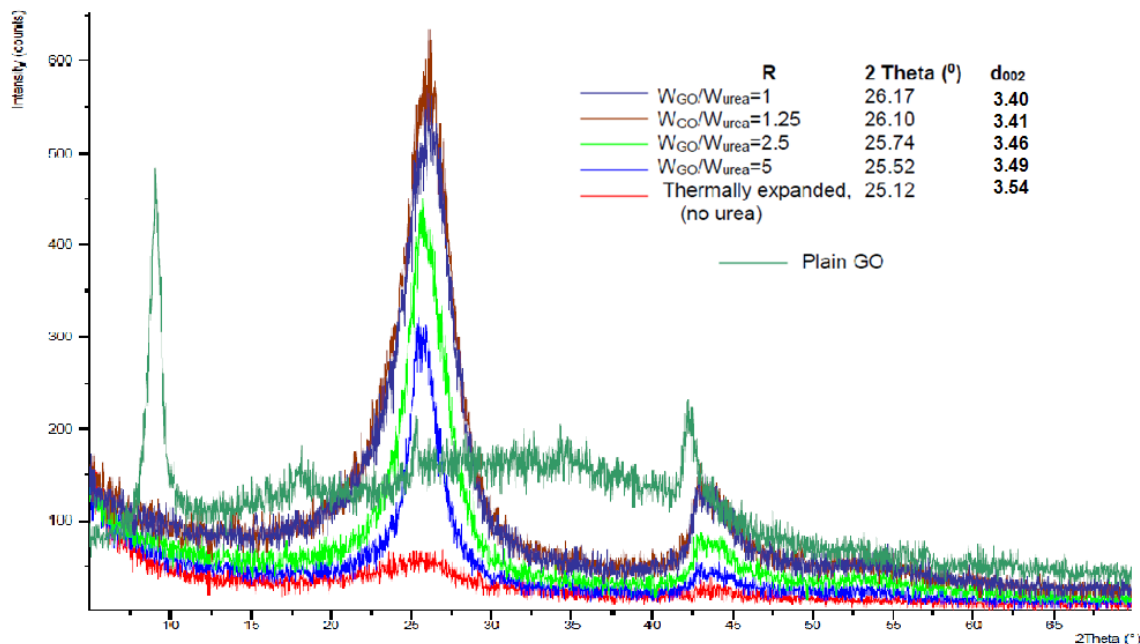


**Figure 18.** XRD results from analysis of all expansion-reduction prepared samples overlaid with thermally expanded (TE) GO without urea and unaltered GO.

Both the primary and secondary peaks are clearly affected by the addition of urea, which suggests that nitrogen has been doped into the graphene. The feature that is of interest is how the (002) peak is shifting along the 2θ axis. For each sample, the addition of urea leads to the peak shifting farther to the right. In other words, the more urea added used in the preparation of graphene, the higher the 2θ value (figure 19 shows in more detail how the peaks were affected by the addition of urea).

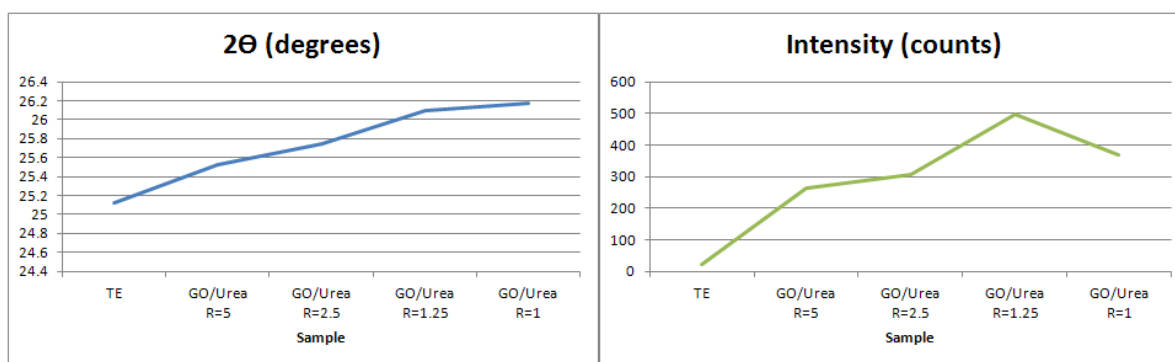


**Figure 19.** On the left: a comparison of various sample’s primary peak position. An increase in urea corresponds to a greater shift to the right. On the right: a comparison of various sample’s peak intensity. Intensity reaches a maximum for R=1.25, after which a greater amount of urea leads to a lower intensity. TE for both graphs stands for thermally expanded.

A greater  $2\theta$  value corresponds directly to a smaller d-value, which means less spacing between planes. This is consistent with what we would expect if nitrogen was inserted into the graphene lattice. Nitrogen causes the graphene sheets to attract to each other, decreasing the amount of space in the plane. The results of the ATP prepared samples are shown in figure 20. While it is clear that this method is converting GO into graphene, adding nitrogen to the aerosol mixture does not seem to dope the graphene product with nitrogen. Another important feature in this figure is the sharp spike that appears in the curve associated with the sample prepared only with argon gas (red). This spike is similar in location along the  $2\theta$  axis to the spike that appears in the unaltered GO sample. This suggests that some of the ATP argon gas sample contains some amount of GO. It is possible during the ATP process that some GO passed through the plasma too quickly to be expanded. Subsequent characterization of this sample also shows evidence that GO is present (described in later sections).

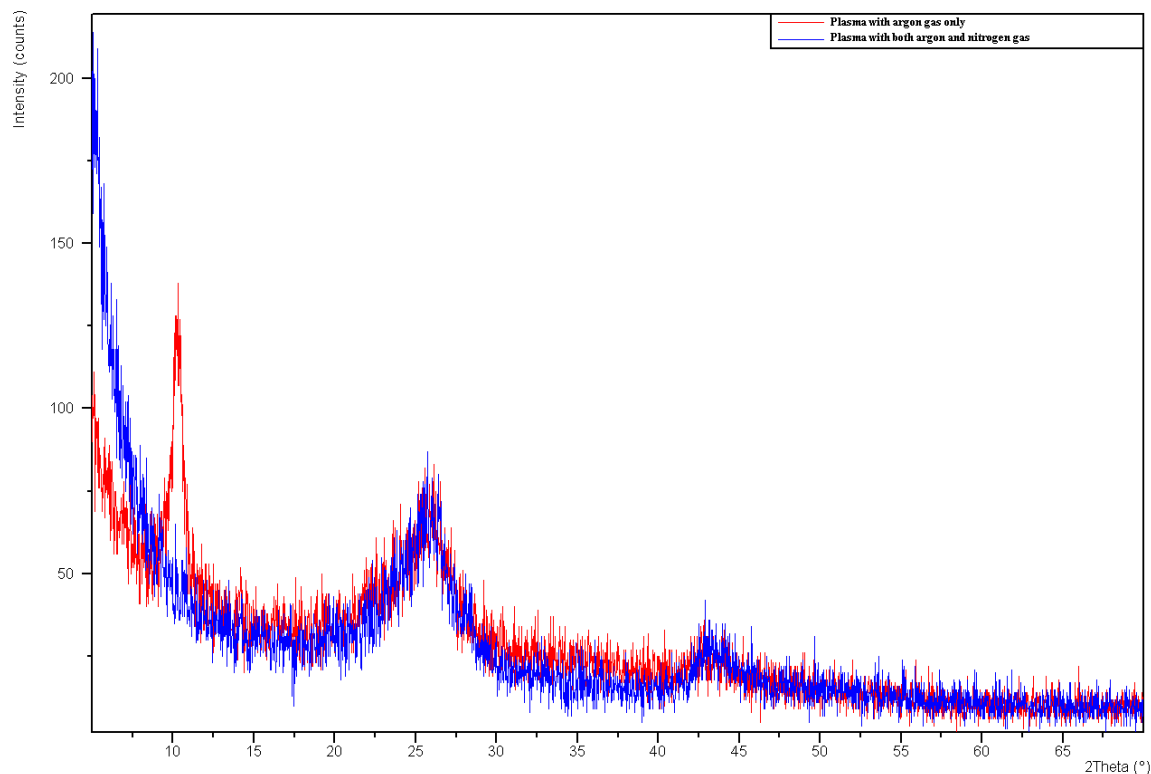


**Figure 20.** XRD results for both ATP prepared samples. The primary peak that occurs at  $26^\circ$   $2\theta$  is unaltered even after adding nitrogen in aerosol mixture. This suggests that no nitrogen was inserted into the resultant graphene.

These results give us feedback in regard to the experimental conditions used. For future runs, we will need to keep carrier gas flows at lower rates than those used in these ATP samples.

## B. BET ANALYSIS

Figure 21 displays how surface area in the expansion-reduction prepared graphene changes depending on how much urea was added. Increasing urea corresponds to decreasing surface area. We believe this might be because of the free electrons that nitrogen introduces into the graphene lattice. The electrons cause the self-standing graphene sheets to attract to each other, reducing the overall surface area of the material. Even with a GO:Urea ratio of five-to-one ( $R=5$ ), there is a dramatic cut in surface area. This is consistent with the hypothesis that nitrogen is has been added to the graphene lattice and that nitrogen causes a loss of surface area.

This information, along with the electrical conductivity of the samples, will help determine what the ideal amount of nitrogen is in order to produce an electrode material with the greatest ability to store energy in ultracapacitor devices.

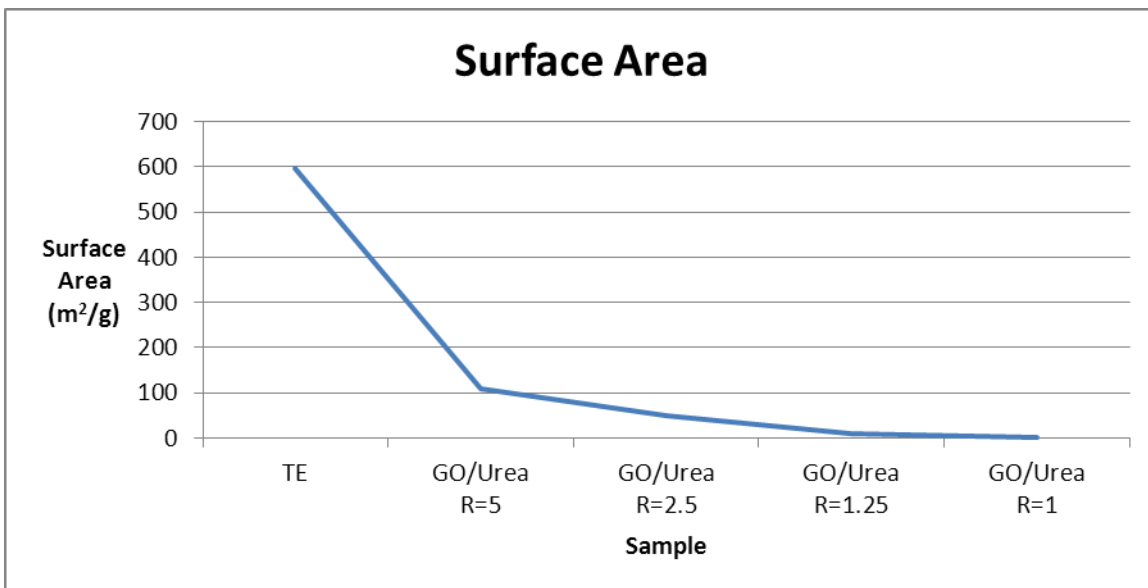


**Figure 21.** Comparison of surface area for different expansion-reduction prepared samples. The thermally expanded (TE) sample, in which no urea was used, shows the largest surface area.

The ATP sample prepared with nitrogen gas showed an increase in surface area versus the ATP sample prepared with only argon gas. This is most likely because non-exfoliated GO is present in the argon gas sample.

The implications of a reduced surface area in graphene as a result of nitrogen doping will be discussed in Chapter V.

### **C. RAMAN SPECTROSCOPY**

There are two principle peaks that are observed in disordered carbon materials that are of interest to us. One is referred to as the G band. We observed this peak at roughly  $1600\text{ cm}^{-1}$  for the samples tested, which is consistent with what other researchers have found [46]. Researchers have observed differences in G band frequencies when comparing graphite, GO and graphene [47]. However, it should be stressed that the differences in these G band frequencies were very minor and other researchers have found that the G band intensities for graphene and graphite are comparable [48]. The reason why the G band is so similar in both frequency and intensity across so many different forms of carbon is that it relies on the bond-stretching motion of  $sp^2$ -bonded C atom pairs [46].

The other band that is of interest to us is the D band (also known as the double-resonant band). We observed the D band to peak around  $1360\text{ cm}^{-1}$ , which is similar to previous research [48]. The D band behaves differently than the G band. Unlike, the G band, the D band is only observed with the presence of sixfold rings, but also requires the presence of a defect to become Raman active. This makes the D band very sensitive to the presence of impurities in the graphene lattice. Unlike the G band, the D band is dispersive, meaning its intensity varies with photon excitation energy [46].

In order to compare the relative intensity ratio of the two bands for different graphene samples, a Lorentzian-Gaussian mix fit was used. As can be seen in figure 22 (which compares the samples prepared with the expansion-reduction method), the D-band-to-G band (D/G) intensity ratio increases with an increase in the amount of urea used in the sample preparation. This is direct evidence for successful nitrogen doping as nitrogen can be considered a defect in the honeycomb lattice. However, there is an

important thing to note about the unaltered GO curve. It appears uncharacteristic when compared to the graphene curves and GO curves found in other research [47]. This is because the signal was overshadowed by a strong luminescent background.

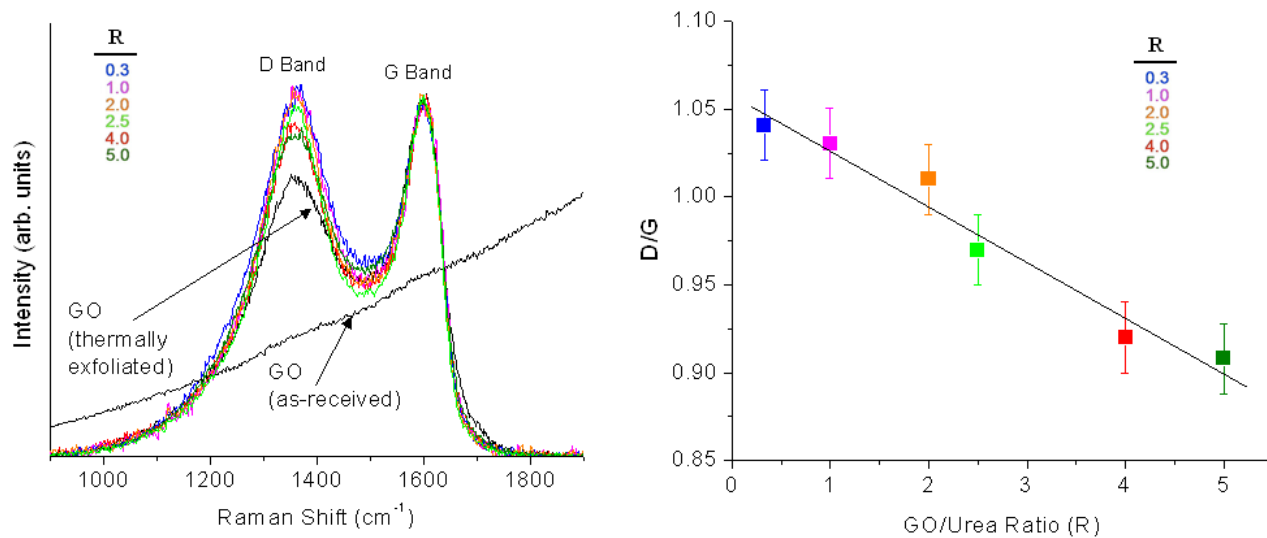


**Figure 22.** On the left: Raman spectrum showing the D/G ratio of various nitrogen-doped samples. On the right: graph showing a relatively linear relationship between D/G ratio and GO:Urea ratio.

Unfortunately, the samples prepared under the ATP method proved to be too inhomogeneous for any valid comparison.

#### D. SCANNING ELECTRON MICROSCOPE

Two images of graphitic oxide are shown in figure 23.

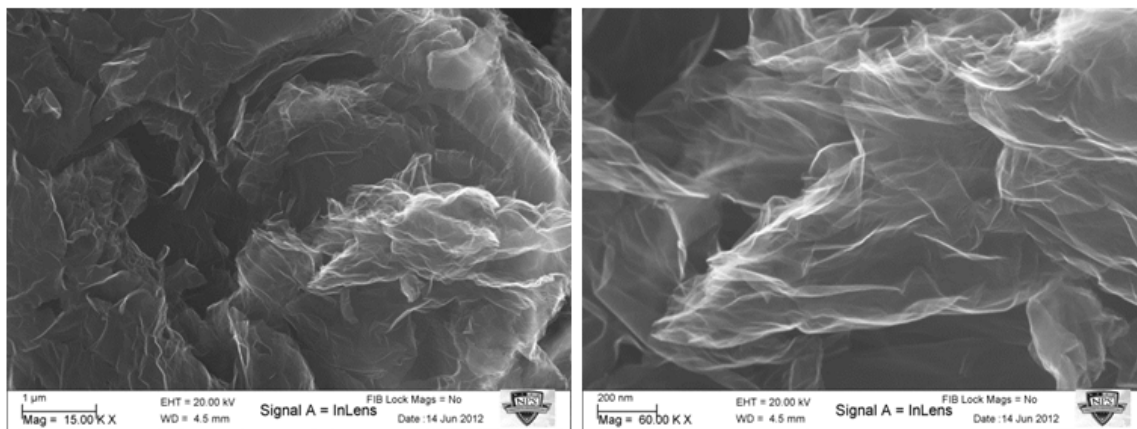


**Figure 23.** Two SEM images of unaltered GO. Image on left is at 15K magnification. Image on right is at 60K magnification.

This images show a fairly voluminous material. This is expected due to the oxygen groups that are present between the graphite sheets. Figure 24 is an SEM image of thermally expanded GO without any urea used in its preparation. The thermally expanded GO also displays voluminous characteristics even though most of the oxygen was removed.

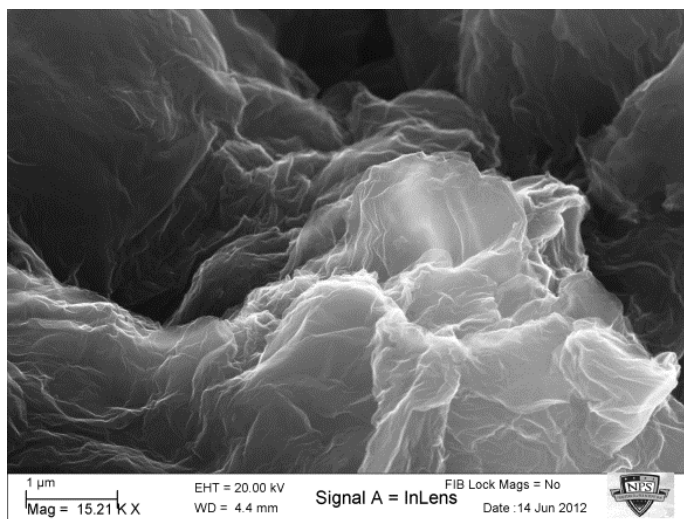


**Figure 24.** SEM images of thermally expanded GO at 15K. Like the unaltered GO, it shows a somewhat loose configuration even though most of the oxygen has been removed.

As explained earlier, introducing nitrogen into a graphene lattice causes the self-standing graphene sheets to become more attracted to one another. This would produce a more compact graphene image. As one can observe in figure 25, the SEM images are showing a tighter clumping for samples with a greater ratio of urea used in their preparation.

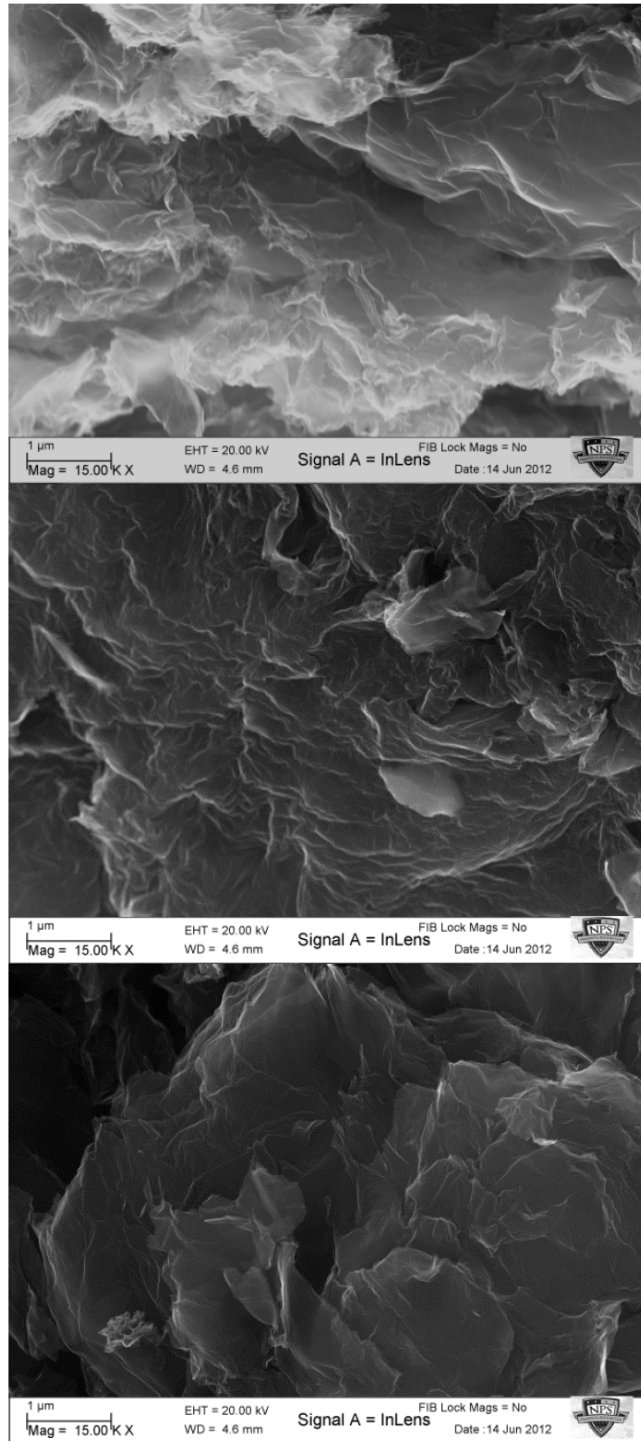


**Figure 25.** SEM images of three different graphene samples. From top to bottom: R=1.67, R=1.25 and R=1. All images are at 15K magnification.

SEM images seem to confirm that nitrogen is being added to graphene through our preparation technique.

### E. THERMOGRAVIMETRIC ANALYSIS

The TGA results showed a lower burn-off temperature for the ATP samples and the thermally expanded (TE) sample (prepared with no urea) versus the samples prepared with the expansion-reduction method with urea. This means that samples are more stable in oxygen containing atmospheres when they are doped. All samples were stable up to 450° C. However, there was no strong correlation among the expansion-reduction samples in relation to the amount of urea used (see figure 26).

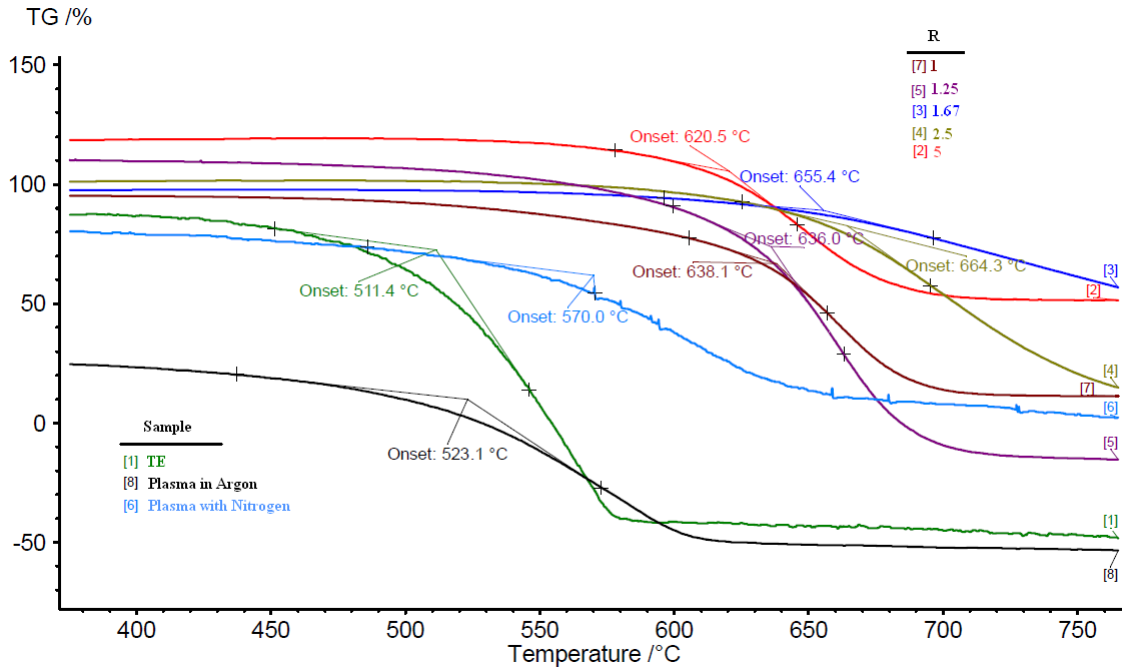


**Figure 26.** TGA graph showing samples produced from both the expansion-reduction method and the ATP method. The thermally expanded (TE) sample (which was prepared with no urea) and the ATP samples were burned off at a lower temperature than the expansion-reduction samples prepared with urea. All samples were stable up to at least 450° C.

An interesting feature to note about the ATP sample prepared with only argon gas is that it exhibits a step pattern for its burn-off rate (see figure 27). This step pattern is similar to what other researchers have observed in TGA characterizations of unaltered GO [49]. This is further evidence that some GO went through the ATP preparation without being exfoliated.

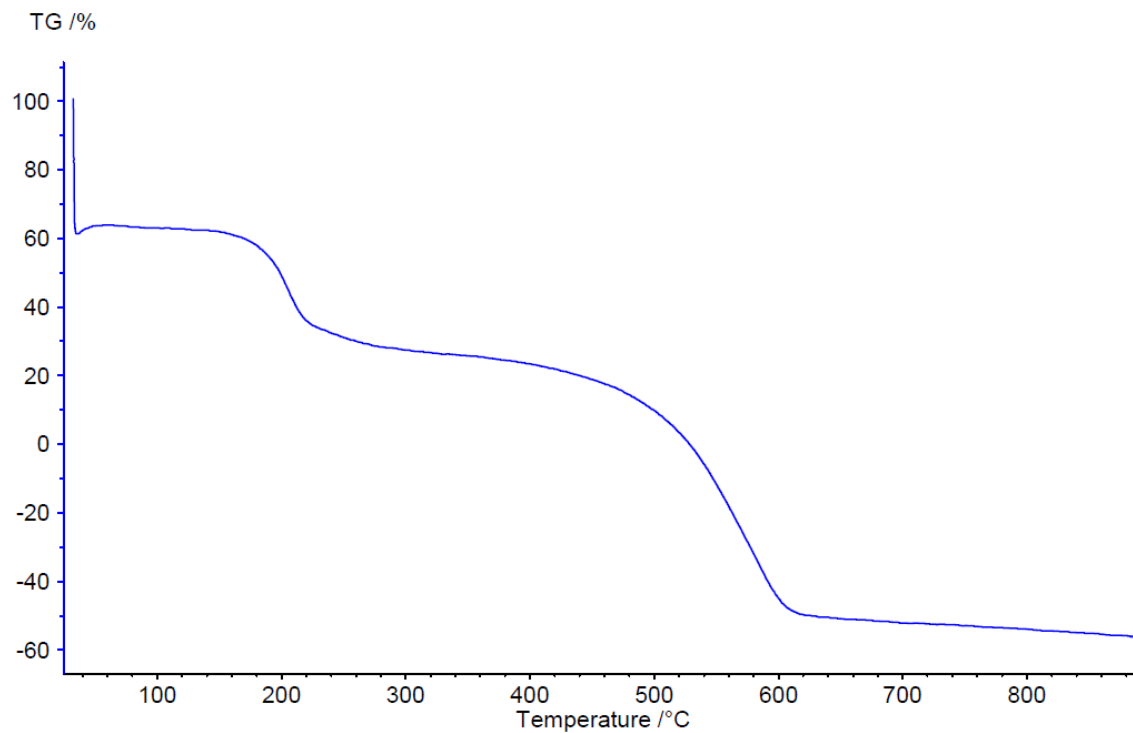


**Figure 27.** TGA graph of ATP sample prepared with argon gas only. The step-down shape is characteristic of unaltered GO.

## F. MASS SPECTROSCOPY

The mass spectroscopy analysis presented unique challenges. Different masses are presented with different intensities but without any clear indication as to what molecules supplied those masses. In order to give the reader an idea of what raw data from a mass spectroscopy run looks like, a typical chart is shown in figure 28.

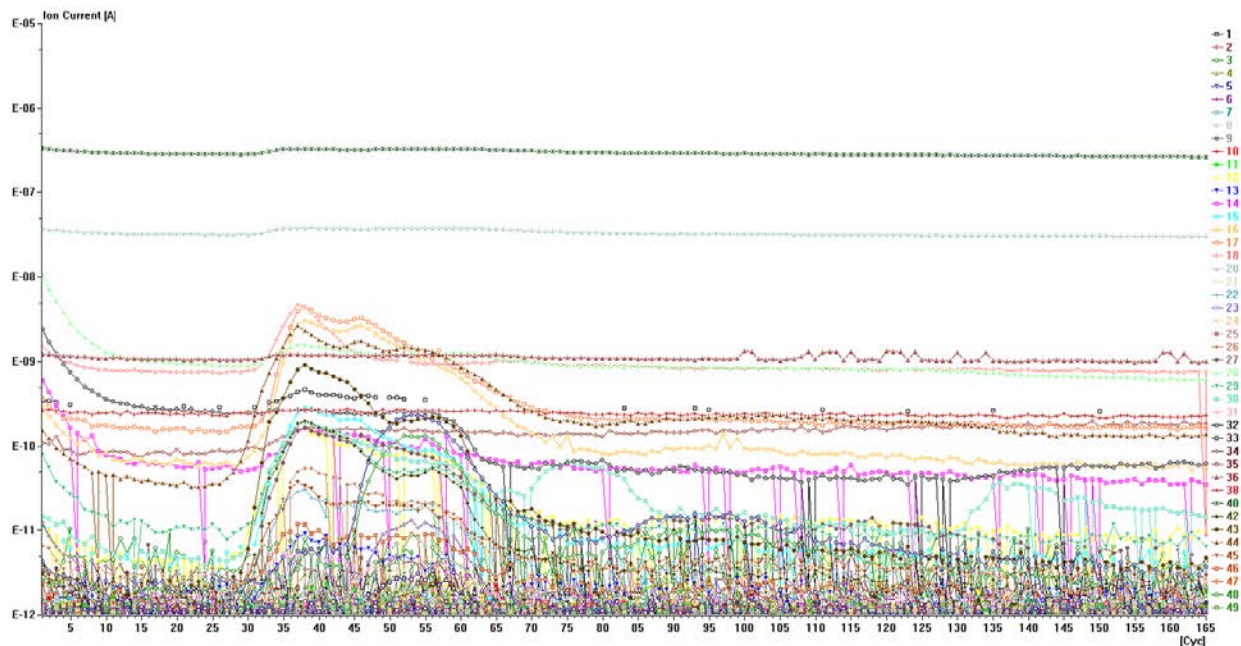


**Figure 28.** Mass Spectra graph for expansion-reduction sample with an R value of 1 (equal parts GO and urea).

Ion current is plotted on the Y-axis and cycles (representative of time) on the X-axis. Each line represents a different mass. What makes a mass significant, however, is not its *absolute* intensity, but rather how it is different from its baseline. For example, in figure 28 masses 20 and 40 have two of the highest overall intensities, but are relatively flat throughout the test. Thus, mass 20 and mass 40 are of little interest to us. However, mass 16, even with a lower overall intensity, shows a large, noticeable spike from its baseline. Mass 16, therefore, is a mass of interest.

Masses that show little or no changes over the course of the mass spectra run are removed (one-by-one) from the chart until masses that show noticeable differences remain. This is done for each individual sample. Then, we want to compare masses associated with nitrogen molecules to the masses associated with carbon molecules. If nitrogen molecule masses are more abundant in a sample versus carbon molecule masses, meaning more nitrogen was in the sample.

However, another problem rises at this point. Many of the masses associated with nitrogen molecules are also associated with carbon molecules. For instance, masses 14 and 16, while both showing large relative spikes, are associated with nitrogen molecules

like NO and NO<sub>2</sub>. Unfortunately, those same masses also exist in molecule like CO and CO<sub>2</sub>. We would expect to see all of these gases from a mass spectra analysis. It is unclear how much nitrogen molecules contribute to these relative intensities.

Not many masses are exclusively associated with one element or the other. Ultimately, the mass spectra analysis focused on only two masses: 30 and 44. Mass 30 is found almost exclusively in nitrogen molecules and mass 44 is almost exclusively associated with carbon molecules. Mass 30 was measured as a percentage of mass 44 in all samples (see figure 29). There appears to be a loose correlation between the Mass 30/Mass 44 intensities and the amount of urea used in the sample. This suggests that using more urea increases the concentration of nitrogen being inserted into the graphene lattice.

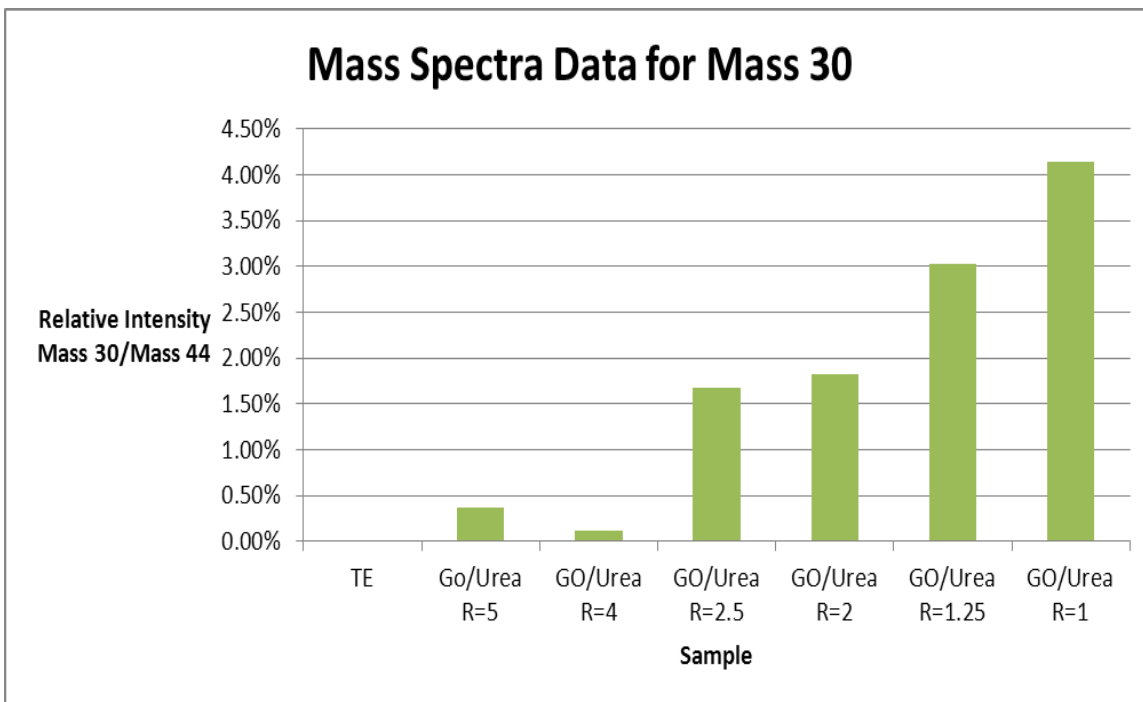


**Figure 29.** Chart showing how much of mass 30 is present in a sample relative to how much of mass 44 is present. There appears to be a loose correlation between the relative amount of Mass 30 (associated with nitrogen molecules) in a sample and the amount of urea used in that sample's preparation.

THIS PAGE INTENTIONALLY LEFT BLANK

## V. SUMMARY AND CONCLUSIONS

This study proved the efficacy of the expansion-reduction method for inserting nitrogen into graphene in a controlled manner, confirming our hypothesis. Indeed, urea mixtures with graphitic oxide will promote the exfoliation of the GO layers while producing reducing gases that will reduce amounts of oxygen groups to minimal levels and also insert nitrogen in the graphene structure.

While plasma based synthesis of graphene was conducted, no evidence of nitrogen doping was present for the ATP method products under the conditions we used. ATP may be effective if conditions are altered or urea is also introduced as precursor.

We also confirmed (using SEM, XRD, mass and Raman spectroscopy) the samples were structurally modified (sheet separation, peak shift due to sheet interaction and d-spacing modification) and confirmed nitrogen was being inserted. Raman spectroscopy, because of the strong dependence between peak D and G intensities, may be the best way to characterize nitrogen additions in future studies.

Samples stability in oxygen containing atmospheres shows that samples are stable up to (at least) 450° C. Higher stabilities are seen for doped samples. It is believed that the extra electrons introduced by nitrogen promote the attraction between graphene sheets. Surface area analysis (by BET) showed that samples have large surface areas as prepared (approx. 600 m<sup>2</sup>/g). Values were drastically reduced as more nitrogen was introduced into the graphene lattice. The effect is even visible with the naked eye since samples volumes decrease proportionally.

Unfortunately, this loss of surface area is undesirable. As explained earlier, a smaller surface area will reduce how many ions in an electrolyte can cling to the surface of an ultracapacitor's electrodes. The surface area reduction will, at least partially, mitigate gains made from the increased conductivity nitrogen doping should offer. It is unclear which effect will dominate. The next steps for continuing this research would be to test the conductivity of the different graphene samples and then test the materials as ultracapacitor electrodes. It may be that there is an ideal level of nitrogen doping where

the gains made from increased conductivity (from the extra charge carriers that nitrogen provides) no longer overcome the loss of surface area.

THIS PAGE INTENTIONALLY LEFT BLANK

## LIST OF REFERENCES

- [1] Committee on Autonomous Vehicles in Support of Naval Operations, National Research Council, "Autonomous vehicles in support of naval operations," The National Academies Press, Washington, D.C., 2005.
- [2] Department of the Navy, "The navy unmanned undersea vehicle (uuv) master plan," November 9, 2004.
- [3] M. D. Stoller, S. Park, Y. Zhu, J. An, and R. S. Ruoff, "Graphene-based ultracapacitors," *Nano Letters*, vol. 8, pp. 3498-3502, 2008.
- [4] J. Garthwaite, "How ultracapacitors work (and why they fall short)," *Gigaom* [Online]. Available: <http://gigaom.com/cleantech/how-ultracapacitors-work-and-why-they-fall-short/>, July 12, 2011.
- [5] Y. Zhu, S. Murali, M. D. Stoller, K. J. Ganesh, W. Cai, P. J. Ferreira, A. Pirkle, R. M. Wallace, K. A. Cychosz, M. Thommes, D. Su, E. A. Stach, and R. S. Ruoff, "Carbon-based supercapacitors produced by activation of graphene," *Science*, vol. 332, pp. 1537-1541, 2011.
- [6] S. Lo, "Energy storage device: ultra-capacitor," Orlando: *University of Central Florida*.
- [7] L. Lai, L. Chen, D. Zhan, L. Sun, J. Liu, S. H. Lim, C. K. Poh, Z. Shen, and J. Lin, "One-step synthesis of nh<sub>2</sub>-graphene from *in situ* graphene-oxide reduction and its improved electrochemical properties," *Carbon*, vol. 49, pp. 3250-3257, 2011.
- [8] Woodbank Communications Ltd. "Ragone plot," Internet: <http://www.mpoweruk.com/performance.htm>, 2005 [July 15, 2012].
- [9] D. Halber. Researchers fired up over new battery. Presented at *15th International Seminar on Double Layer Capacitors and Hybrid Energy Storage Devices*. Deerfield Beach, Florida, 2005.
- [10] S. Stankovich, D. A. Dikin, G. H. B. Dommett, K. Kohlhaas M., E. J. Zimmey, E. A. Stach, R. D. Piner, S. T. Nguyen, and R. S. Ruoff, "Graphene-based composite materials," *Nature*, vol. 442, pp. 282-286, 2006.
- [11] A. C. Dillon, "Carbon nanotubes for photoconversion and electrical energy storage," *Chemical Reviews*, vol. 110, pp. 6856-6872, September 14, 2010.

- [12] E. J. Lerner, "Less is more with aerogels," *The Industrial Physicist*, vol. 10, pp. 26-30, September 21, 2004.
- [13] M. Arulepp, J. Leis, M. Latt, F. Miller, K. Rumma, E. Lust, and A. F. Burke, "The advanced carbide-derived carbon based supercapacitor," *Journal of Power Sources*, vol. 162, pp. 1460-1466, November 22, 2006.
- [14] A. K. Geim and K. S. Novoselov, "The rise of graphene," *Nature Materials*, vol. 6, pp. 183-191, March 2007.
- [15] I. W. Frank, D. M. Tanenbaum, van der Zande, A. M., and P. L. McEuen, "Mechanical properties of suspended graphene sheets," *Journal of Vacuum Science and Technology B: Microelectronics and Nanometer Structures*, vol. 25, pp. 2558-2561, 2007.
- [16] G. D. Stucky, "High surface area materials," Internet: [http://www.wtec.org/loyola/nano/us\\_r\\_n\\_d/07\\_03.htm](http://www.wtec.org/loyola/nano/us_r_n_d/07_03.htm), January 1998 [March 8, 2012].
- [17] C. Liu, Z. Yu, D. Neff, A. Zhamu, and B. Z. Jang, "Graphene-based supercapacitor with an ultrahigh energy density," *Nano Letters*, vol. 10, pp. 4863-4868, November 8, 2010.
- [18] Y. Wang, Y. Shao, D. W. Matson, J. Li, and Y. Lin, "Nitrogen-doped graphene and its application in electrochemical biosensing," *ACS Nano*, vol. 4, pp. 1790-1798, April 7, 2010.
- [19] M. Balkanski and R. F. Wallis, *Semiconductor Physics and Applications*. New York: Oxford University Press, 2000.
- [20] B. Guo, L. Fang, B. Zhang, and J. R. Gong, "Graphene doping: a review," *Insciences Journal*, vol. 1, pp. 80-89, April 27, 2011.
- [21] A. K. Geim and P. Kim, "Carbon wonderland: graphene, a newly isolated form of carbon, provides a rich lode of novel fundamental physics and practical applications," *Scientific American*, vol. 8, pp. 90-97, March 17, 2008.
- [22] A. K. Geim and A. H. MacDonald, "Graphene: exploring the carbon flatland," *Physics Today*, vol. 60, pp. 35-41, August 2007.
- [23] X. Liu, T. H. Metcalf, J. T. Robinson, B. H. Houston, and F. Scarpa, "Shear modulus of monolayer graphene prepared by chemical vapor deposition," *Nano Letters*, vol. 12, pp. 1013-1017, January 3, 2012.
- [24] X. Li, W. Cai, J. An, S. Kim, J. Nah, D. Yang, R. Piner, A. Velamakanni, I. Jung, E. Tutuc, S. Banerjee, L. Colombo, and R. Ruoff, "Large-area synthesis of high-

- quality and uniform graphene films on copper foils," *Science*, vol. 324, pp. 1312-1314, June 5, 2009.
- [25] Z. Sun, Z. Yan, J. Yao, E. Beitler, Y. Zhu, and J. Tour, "Growth of graphene from solid carbon sources," *Nature*, vol. 468, pp. 549-552, November 25, 2010.
- [26] P. Stutter, "Epitaxial graphene: how silicon leaves the scene," *Nature Materials*, vol. 8, pp. 171-172, 2009.
- [27] P. Stutter, J. Flege, and E. Stutter, "Epitaxial graphene on ruthenium," *Nature Materials*, vol. 7, pp. , April 6, 2008.
- [28] J. Coraux, A. N'Diaye, M. Engler, C. Busse, D. Wall, N. Buckanie, F. Heringdorf, R. van Gastel, B. Poelsema, and T. Michely, "Growth of graphene on ir(111)," *New Journal of Physics*, vol. 11, pp. 1-22, February 4, 2009.
- [29] H. P. Boehm, A. Clauss, G. Fischer, and U. Hofman, "Surface properties of extremely thin graphite lamellae," in *Proceedings of the Fifth Conference on Carbon*, Heidelberg, Germany, 1962, .
- [30] S. Wakeland, R. Martinez, J. K. Grey, and C. C. Luhrs, "Production of graphene from graphite oxide using urea as expansion-reduction agent," *Carbon*, vol. 48, pp. 3463-3470, 2010.
- [31] D. C. Marcano, D. V. Kosynkin, J. M. Berlin, A. Sinitskii, Z. Sun, A. Slesarev, L. B. Alemany, W. Lu, and J. M. Tour, "Improved synthesis of graphene oxide," *ACS Nano*, vol. 4, pp. 4806-4814, July 22, 2010.
- [32] A. Dato, V. Radmilovic, Z. H. Lee, J. Phillips, and M. Frenklach, "Substrate-free gas-phase synthesis of graphene sheets," *Nano Letters*, vol. 8, pp. 2012-2016, 2008.
- [33] T. N. Lambert, C. C. Luhrs, C. A. Chavez, S. Wakeland, M. T. Brumach, and T. M. Alam, "Graphite oxide as a precursor for the synthesis of disordered graphenes using the aerosol-through-plasma method," *Carbon*, vol. 48, pp. 4081-4089, 2010.
- [34] B. D. Cullity, *Elements of X-Ray Diffraction*. Addison-Wesley Pub. Co. Inc, 1978.
- [35] S. Brunauer, P. H. Emmett, and E. Teller, "Adsorption of gases in multimolecular layers," *Journal of the American Chemistry Society*, vol. 60, pp. 309-319, February 1938.

- [36] N. Hwang and A. Barron, "bet surface area analysis," *Connexions* [Online]. Available: <http://cnx.org/content/m38278/latest/?collection=col10699/latest>, May 8, 2011 [18 April 2012].
- [37] Quantachrome Instruments, "novae series high-speed surface area and pore size analyzers," Internet: [http://www.quantachrome.com/pdf\\_brochures/07122.pdf](http://www.quantachrome.com/pdf_brochures/07122.pdf) 2011, [16 April 2012].
- [38] E. C. Le Rue and P. G. Etchegoin, "Chapter 2: raman spectroscopy and related optical techniques," in *Principles of Surface-Enhanced Raman Spectroscopy and Related Plasmonic Effects* Anonymous Elsevier, 2009, pp. 29-120.
- [39] Princeton Instruments, "Raman spectroscopy basics," Internet: [http://content.piacron.com/Uploads/Princeton/Documents/Library/UpdatedLibrary/Raman\\_Spectroscopy\\_Basics.pdf](http://content.piacron.com/Uploads/Princeton/Documents/Library/UpdatedLibrary/Raman_Spectroscopy_Basics.pdf), 2012 [15 June 2012].
- [40] J. Reintjes and M. Bashkansky, "Chapter 15: stimulated raman and brillouin scattering," in *Handbook of Optics, Volume IV - Optical Properties of Materials, Nonlinear Optics, Quantum Optics*, 3rd ed., M. Bass, G. Li and E. V. Stryland, Eds. McGraw-Hill, 2010, pp. 15.1-15.60.
- [41] S. Swapp, "Scanning electron microscopy (sem)," Internet: [http://serc.carleton.edu/research\\_education/geochemsheets/techniques/SEM.html](http://serc.carleton.edu/research_education/geochemsheets/techniques/SEM.html), [July 23, 2012].
- [42] B. L. Gabriel, *SEM: A User's Manual for Materials Science*. Metals Park, OH: American Soceiety for Metals, 1985.
- [43] PerkinElmer, Inc. "A beginner's guide to thermogravimetric analysis," Internet: [http://www.perkinelmer.com/CMSResources/Images/44-74556GDE\\_TGA\\_BeginnersGuide.pdf](http://www.perkinelmer.com/CMSResources/Images/44-74556GDE_TGA_BeginnersGuide.pdf), 2010 [15 June 2012].
- [44] S. Higson, "Chapter 9: mass spectrometry," in *Analytical Chemistry* Anonymous New York: Oxford University Press, 2004, pp. 247.
- [45] NETZSCH Group, "New dimensions in gas analysis: qms 403 c aeolos - quadrupole mass spectrometer," Internet: <http://www.netzsch-thermal-analysis.com/en/products/detail/pid,33.html>, [14 June 2012].
- [46] A. C. Ferrari and J. Robertson, "Interpretation of raman spectra of disordered and amorphous carbon," *The American Physical Society*, vol. 61, pp. 14095-14107, May 15, 2000.

- [47] K. Kudin N., B. Ozbas, H. C. Schniepp, R. K. Prud'homme, I. A. Aksay, and R. Car, "Raman spectra of graphite oxide and functionalized graphene sheets," *Nano Letters*, vol. 8, pp. 36-41, January 9, 2008.
- [48] A. C. Ferrari, J. C. Meyer, V. Scardaci, C. Casiraghi, M. Lazzeri, F. Mauri, S. Piscanec, D. Jiang, K. S. Novoselov, S. Roth, and A. K. Geim, "raman spectrum of graphene and graphene layers," *Physical Review Letters*, vol. 97, pp. 1874011-1874014, November 3, 2006.
- [49] J. P. Rourke, P. A. Pandey, J. J. Moore, M. Bates, I. A. Kinloch, R. J. Young, and N. R. Wilson, "The real graphene oxide revealed: stripping the oxidative debris from the graphene-like sheets," *Angewandte Chemie International Edition*, vol. 50, pp. 3173-3177, 2011.

THIS PAGE INTENTIONALLY LEFT BLANK

## INITIAL DISTRIBUTION LIST

1. Defense Technical Information Center  
Ft. Belvoir, Virginia
2. Dudley Knox Library  
Naval Postgraduate School  
Monterey, California
3. Claudia Luhrs  
Naval Postgraduate School  
Monterey, California
4. Sebastian Osswald  
Naval Postgraduate School  
Monterey, California